## Journal Pre-proof

Engineered *Lactococcus lactis* Biovaccine Containing NY-ESO-1 Long Peptides as Potent Immunotherapeutics

Chunyi Li, Kongcheng Wang, Jie Shao, Junmeng Zhu, Yaohua Ke, Baorui Liu, Lanqi Cen

Bu dave so del fortuna pla Pero

materialstoday

PII: S2590-0064(25)01011-7

DOI: https://doi.org/10.1016/j.mtbio.2025.102440

Reference: MTBIO 102440

To appear in: Materials Today Bio

Received Date: 24 June 2025

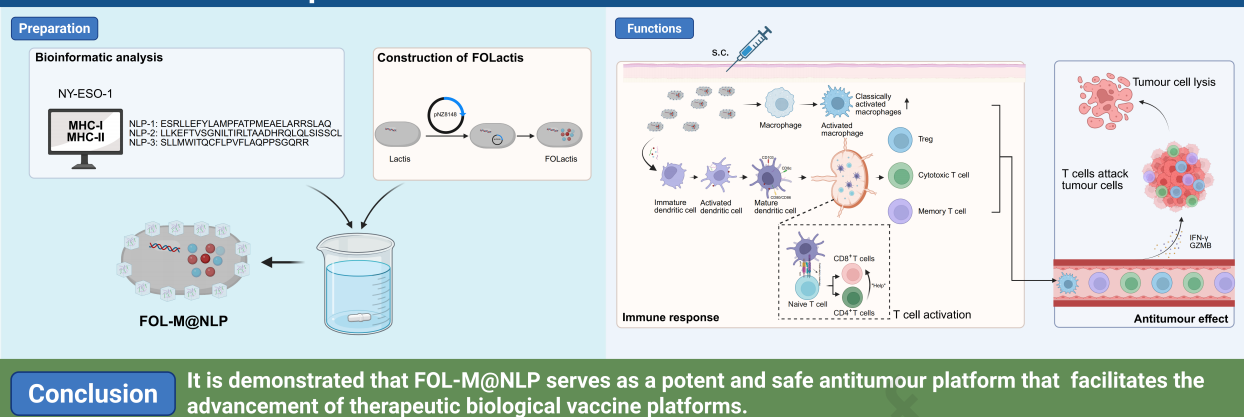
Revised Date: 17 October 2025 Accepted Date: 19 October 2025

Please cite this article as: C. Li, K. Wang, J. Shao, J. Zhu, Y. Ke, B. Liu, L. Cen, Engineered *Lactococcus lactis* Biovaccine Containing NY-ESO-1 Long Peptides as Potent Immunotherapeutics, *Materials Today Bio*, https://doi.org/10.1016/j.mtbio.2025.102440.

This is a PDF file of an article that has undergone enhancements after acceptance, such as the addition of a cover page and metadata, and formatting for readability, but it is not yet the definitive version of record. This version will undergo additional copyediting, typesetting and review before it is published in its final form, but we are providing this version to give early visibility of the article. Please note that, during the production process, errors may be discovered which could affect the content, and all legal disclaimers that apply to the journal pertain.

© 2025 Published by Elsevier Ltd.

# Engineered *Lactococcus lactis* Biovaccine Containing NY-ESO-1 Long Peptides as Potent Immunotherapeutics



#### Engineered Lactococcus lactis Biovaccine Containing NY-1

#### **ESO-1** Long Peptides as Potent Immunotherapeutics 2

3 4

Chunyi Li<sup>1</sup>, Kongcheng Wang<sup>2</sup>, Jie Shao<sup>2</sup>, Junmeng Zhu<sup>2</sup>, Yaohua Ke<sup>2</sup>, Baorui Liu<sup>1, 2,</sup>

<sup>3\*</sup>, Lanqi Cen<sup>2</sup>\* 5

6

- <sup>1</sup> Department of Oncology, Nanjing Drum Tower Hospital Clinical College of Nanjing 7
- Medical University, Nanjing, China. 210000. 8
- <sup>2</sup> Department of Oncology, Nanjing Drum Tower Hospital, Affiliated Hospital of 9
- Medical School, Nanjing University, Nanjing, China. 210000. 10
- <sup>3</sup> Department of Oncology, Nanjing Drum Tower Hospital and Group's Sugian Hospital, 11
- Affiliated Hospital of Medical School, Nanjing University, Nanjing, China. 210000. 12

13

- \*Corresponding authors: 14
- 15 Langi Cen, Department of Oncology, Nanjing Drum Tower Hospital, Affiliated
- Hospital of Medical School, Nanjing University, Nanjing, China. E-mail: 16
- 17 lqcjsnj05@163.com

18

- 19 Baorui Liu, Department of Oncology, Nanjing Drum Tower Hospital Clinical College
- of Nanjing Medical University, Nanjing, China. E-mail: baoruiliu@nju.edu.cn 20

21

#### Abstract

23

24

25

26

27

28

29

30

31

32

33

34

35

36

37

38

39

40

41

42

43

44

Peptide vaccines have potential for tumour immunotherapy but face challenges in clinical trials, such as human leukocyte antigen limitations, potential cytotoxic T lymphocyte tolerance, short T-cell response duration, weak immune response, and other issues. Optimizing the antigens of peptide vaccines and selecting an effective delivery system are crucial for enhancing their antitumour effects. 3 multiepitope long peptides (NLP) targeting the NY-ESO-1 antigen were screened using bioinformatics methods. An engineered Lactococcus lactis strain (FOLactis) expressing FMS-like tyrosine kinase 3 ligand and the costimulator OX40 ligand was previously developed to activate immune cells. In this study, FOLactis was utilized as a biological carrier for NLP via Mg<sup>2+</sup>-based metal-organic frameworks to stimulate innate and adaptive immunity. The FOL-M@NLP were characterized, and various tumour models were established to assess the antitumour efficacy of the biovaccine. The preliminary mechanism of the immune effect induced by FOL-M@NLP was studied both in vivo and in vitro. The biovaccine FOL-M@NLP was effectively taken up by antigen-presenting cells (APCs). APCs were activated, activating the T-cell response. When FOL-M@NLP was administered subcutaneously in vivo, their antitumour activity was superior to that of NLP and FOLactis alone. The biovaccine improved the immune infiltrating state of the tumour microenvironment and metastasis niche, inhibited tumor progression and prevented recurrence. It is demonstrated that FOL-M@NLP serves as a potent and safe antitumour platform that enhances antigen peptide delivery and facilitates the advancement of therapeutic biological vaccine platforms.

45 **Keywords:** Tumour vaccine, NY-ESO-1, Multiepitope long peptide, Engineered bacteria, Immunotherapy.

47

48

49

50

51

52

53

54

55

56

57

58

59

60

61

62

63

64

65

66

#### 1. Introduction

Tumor peptide vaccines are extensively employed for their inexpensive cost, uncomplicated preparation, superior safety, and delivered by multiple carriers. However, their poor immunogenicity and susceptibility to the microenvironment result in suboptimal efficacy in tumor immunotherapy and restrict their clinical application. Two directions to solve this problem are as follows. On the one hand, in the design of synthetic peptides. Peptide vaccines usually consist of epitope peptides with high affinity for human leukocyte antigen (HLA). Typically, short peptides (8–11 amino acids) may not be able to overcome antigenic heterogeneity or the loss of antigen expression within the tumour, thereby failing to induce a strong immune response [1]. Therefore, the cytotoxic effect of CD8<sup>+</sup> T cells is limited, and CD4<sup>+</sup> T cells are difficult to activate. Multiepitope long peptide vaccines contain approximately 20-35 amino acids, which contain more major histocompatibility complex (MHC) I and MHC II epitopes and can activate naive T lymphocytes more effectively, but a sufficiently high dose of peptides must be delivered to avoid the induction of T-cell anergy [1]. New York esophageal squamous cell carcinoma-1 (NY-ESO-1) is an ideal target for the development of long peptide vaccines to treat tumours.

It is expressed only in some immune-privileged organs, mainly the testis and placenta 67 [2, 3]. The expression of NY-ESO-1 has been reported in a wide range of tumours, such 68 69 as myxoid and round cell liposarcoma (89-100%), neuroblastoma (82%), synovial sarcoma (80%), melanoma (46%), ovarian cancer (43%), esophageal cancer (32%), 70 71 lung cancer (13%), colorectal cancer (8%) and breast cancer (7%) [3-5]. On the other hand, the delivery of suitable adjuvants and peptides together proves to be a successful 72 approach for clinical tumour vaccines. Nevertheless, when adjuvants and peptides are 73 mixed directly, they encounter issues like poor physical stability and easy dissociation, 74 75 resulting in uneven formulation and potentially inadequate immune effects. Hence, the use of proper adjuvants and delivery methods is essential to enhance and prolong the 76 immune efficacy of peptides [6, 7]. 77 78 Our team designed a bifunctional engineered Lactococcus lactis (FOLactis), which can deliver the fusion protein of FMS-like tyrosine kinase 3 ligand (Flt3L) and the 79 costimulator OX40 ligand (OX40L) [8]. Lactococcus lactis can act as Toll-like receptor 80 81 (TLR) agonists and trigger long-lasting innate immune responses with its pathogen-82 associated molecular patterns (PAMPs) [9, 10], inhibit tumour growth through its antiproliferative activity, induction of apoptosis and cell cycle arrest, etc. [11]. Flt3L 83 promotes the expansion of conventional dentritic cell 1 (cDC1) [12]. The OX40/OX40L 84 85 signalling axis can upregulate antiapoptotic proteins to maintain T-cell survival; downregulate regulatory signals; promote the secretion of IFN-γ; and maintain immune 86 87 memory [13]. Previous experimental studies have shown the engineered bacteria FOLactis, which can act as a strong immune adjuvant, achieves tumour regression 88

| 89 | mainly by enhancing the innate immune response, promoting dendritic cell (DC)              |
|----|--|
| 90 | maturation and strengthening the cytotoxic T lymphocyte response in the tumour             |
| 91 | microenvironment (TME) [8].  |
| 92 | In this study, through bioinformatics, we screened multiepitope long peptides that target  |
| 93 | NY-ESO-1 (NLP). Afterwards, we developed a metal-organic framework (MOF) and               |
| 94 | constructed a system with FOLactis to deliver NLP (FOL-M@NLP). This system has             |
| 95 | been demonstrated to enhance specific immune responses, change the immune                  |
| 96 | infiltrating state of TME and metastasis niche, and trigger effective antitumour           |
| 97 | activities. These results provide strong support for the development of safe and efficient |
| 98 | tumour peptide vaccines utilizing engineered bacteria (Scheme 1).                          |

100

### 2. Materials and methods

101 2.1. Bacterial strains, cells and animals

FOLactis strain was constructed by our laboratory team and preserved in the laboratory 102 of the Cancer Center of Nanjing University Drum Tower Hospital. FOLactis was 103 incubated in M17 (Solarbio, China) medium containing 0.5% (w/v) glucose and 10 μg 104 mL<sup>-1</sup> chloramphenicol (GM17 medium) at 30°C. When the absorbance of the GM17 105 medium at 600 nm reached 0.5–0.7, nisin was added to the medium at a concentration 106 of 10 ng mL<sup>-1</sup>, and the mixture was subsequently incubated for another 4 h. 107 4T1 breast cancer cells and B16F10 melanoma cells were obtained from the Cell Bank 108 of the Shanghai Institute of Biochemistry and Cell Biology and cultured with medium 109 consisting of 89% RPMI 1640 (Corning, USA), 10% fetal bovine serum (FBS) 110

| L11 | (Beyotime, China), and 1% penicillin and streptomycin (P/S) (Biosharp, China) at 37°C                    |
|-----|--|
| L12 | and 5% CO <sub>2</sub> .   |
| L13 | Bone marrow mesenchymal cells were obtained from the femurs and tibias of                                |
| L14 | C57BL/6J mice. These cells were cultured in medium comprising 89% RPMI 1640, 10%                         |
| L15 | FBS, and 1% P/S at 37°C and 5% CO <sub>2</sub> . To induce differentiation into DCs, the cells           |
| L16 | were treated with rmIL-4 (10 ng mL <sup>-1</sup> , Pepro Tech, USA) and rmGM-CSF (20 ng mL <sup>-1</sup> |
| L17 | <sup>1</sup> , Amoytop, China). The culture medium was changed every 48 h, and on day 8, the             |
| L18 | adherent cells were collected as immature bone marrow-derived dendritic cells                            |
| L19 | (BMDCs).   |
| L20 | C57BL/6J mice and BALB/c mice aged 4-6 weeks were purchased from Huachuang                               |
| L21 | Sino Pharmaceutical Technology Co. Ltd. (China). All animal experimental protocols                       |
| L22 | were approved by the Laboratory Animal Care and Use Committee of the Affiliated                          |
| L23 | Nanjing Drum Tower Hospital of Nanjing University Medical School (2023AE01063).                          |
| L24 |  |
| L25 | 2.2. Prediction of epitopes with affinity for HLA and synthesis of NLP                                   |
| L26 | A comprehensive survey of the HLA class I and II loci was conducted, encompassing                        |
| L27 | 812211 individuals across 31 provinces, autonomous regions, and municipalities in                        |
| L28 | China. 6 HLA-A alleles and 8 HLA-DRB1 alleles were selected to represent the genetic                     |
| L29 | diversity of the Chinese population [14]. The amino acid sequence of NY-ESO-1,                           |
| L30 | identified by accession number CAA05908.1, was retrieved from the NCBI database                          |
| L31 | (https://www.ncbi.nlm.nih.gov/). Candidate epitopes for MHC I were identified via                        |
| L32 | NetMHCpan-4.1 (http://www.cbs.dtu.dk/services/NetMHCpan/) and IEDB                                       |

| L33 | (http://tools.iedb.org/mhci/), whereas the IEDB binding prediction tool                                 |
|-----|---|
| L34 | (http://tools.iedb.org/mhcii/) was utilized for MHC II [15, 16].  |
| L35 | Epitopes with high affinity for multiple MHC I and II alleles were identified as probable               |
| L36 | candidates. The screening criterion included strong binding, defined as an affinity rank                |
| L37 | below 0.5%, with various MHC I molecules. Epitopes with rank values between $0.5\%$                     |
| L38 | and 2% were classified as weak binders. Our selection process prioritized peptides with                 |
| L39 | robust affinity and high scores across multiple prediction tools. Owing to the increased                |
| L40 | promiscuity of peptide binding to MHC class II molecules, the accuracy of MHC-II                        |
| L41 | binding prediction is lower than that of MHC-I binding prediction. Consequently, a                      |
| L42 | broader selection of MHC-II categories is necessary. Epitopes with an affinity rank                     |
| L43 | below 10% for specific MHC-II molecules were chosen. 3 multiepitope long peptides                       |
| L44 | from NY-ESO-1 with favourable binding potential for specific HLA types, covering a                      |
| L45 | broad range of HLA loci, were screened, and the synthesis and validation of the                         |
| L46 | screened peptides were performed by GenScript (Nanjing, China).   |
| L47 |   |
| L48 | 2.3. Detection of peptide affinity to MHC molecules by ELISPOT  |
| L49 | Splenocytes from BALB/c mice and C57BL/6J mice were cultured overnight in AIMV                          |
| L50 | (Invitrogen Gibco, USA) medium containing 0.5% FBS (Invitrogen Gibco, USA),                             |
| L51 | rmIL-4 (20 ng mL <sup>-1</sup> ), and rmGM-CSF (40 ng mL <sup>-1</sup> ) after removal of erythrocytes. |
| L52 | Subsequently, splenocytes were added to 96-well plates at $6 \times 10^5$ cells per well. Each          |
| L53 | screened peptide was introduced into the experimental wells at a concentration of 50                    |

 $\mu g~mL^{\text{--}1},$  then resiquimod (3  $\mu g~mL^{\text{--}1},$  Merck, USA) and LPS (50  $ng~mL^{\text{--}1},$  Merck, USA)

were added to all wells after 4 h. On day 2, all cell culture medium was replaced with AIMV medium containing 10% FBS, 1% P/S, IL-2 (24 IU mL<sup>-1</sup>, Pepro Tech, USA) and IL-7 (50 ng mL<sup>-1</sup>, Pepro Tech, USA). Cells were continuously cultured and medium was substituted halfway every 2 days. On day 13, fresh peptide-pulsed cells were obtained following the procedure outlined for preparation on the first 2 days. On day 14, the previously induced cells (2×10<sup>5</sup> cells per well) and newly peptide-pulsed cells (1×10<sup>5</sup> cells per well) were placed in a 96-well ELISPOT plate pre-coated with IFN-γ and incubated at 37°C for 18–20 hours. According to the instruction, the detection was performed by mouse IFN-γ ELISPOT kit (Dakewe, China). Plates were scanned and analysed by AID ELISPOT Reader (Germany).

## 2.4. Preparation and characterization of FOL-M@NLP

7 mmol 2-methylimidazole (Aladdin, China) was dissolved in 10 mL of double distilled water (ddH<sub>2</sub>O), mixed with 5×10<sup>8</sup> CFU FOLactis and stirred at 400 rpm for 10 min. The mixture was then centrifuged at 5000 rpm for 10 min, and only the precipitate remained. An appropriate amount of NLP solution, 1 mL of 100 μmol mL<sup>-1</sup> magnesium sulfate solution (Yangzhou Zhongbao Pharmaceutical Co. Ltd. China) and ddH<sub>2</sub>O were added to the precipitate, and the mixture was stirred at 400 rpm for 20 min. The precipitate remaining after centrifugation was FOL-M@NLP. When no peptide was added during the reaction and only magnesium sulfate was added, the precipitate obtained after centrifugation was FOL-M.

| 177 | 2.5. Cytotoxicity studies  |
|-----|--|
| 178 | FOL-M+NLP (physical mixture of FOL-M and 3 selected peptides, NLP concentration                      |
| 179 | 50 μg mL <sup>-1</sup> ) and FOL-M@NLP were coincubated with 5000 BMDCs at different                 |
| 180 | concentrations of FOLactis for 24 h. Then, 10 µL of sterile CCK-8 reagent (Biosharp,                 |
| 181 | China) was added to each well and incubated at 37°C. The absorbance of each well was                 |
| 182 | measured with a microplate reader. Cell viability was calculated via the following                   |
| 183 | formula:   |
| 184 | Cell viability(%)= $(A_E-A_B)/(A_C-A_B)\times 100\%$   |
| 185 | $A_{\rm E}$ (Experimental group): the absorbance of cells with drugs; $A_{\rm B}$ (Blank group): the |
| 186 | absorbance of medium; $A_{\mathbb{C}}$ (Control group): the absorbance of cells in medium without    |
| 187 | drugs.   |
| 188 |  |
| 189 | 2.6. Detection of cellular uptake  |
| 190 | NLP-3 was labelled with Cy5-NHS (Duofluor, China), and then FOL-M@NLP-3-Cy5                          |
| 191 | was prepared. Flow cytometry was used to detect BMDC phagocytosis of FOL-                            |
| 192 | M@NLP-3-Cy5 and NLP-3-Cy5 at different time points. In addition, NLP-3-Cy5 and                       |
| 193 | FOL-M@NLP-3-Cy5 were coincubated with immature BMDCs. After 2 h, the BMDC                            |
| 194 | membrane was stained with DiO (Beyotime, China), and the BMDC nucleus was                            |
| 195 | stained with DAPI (Beyotime, China). Colocalization of the two irritants and BMDCs                   |
| 196 | was observed via confocal laser scanning microscopy (Leica, Germany).                                |
| 197 |  |
|     |  |

| 199 | Immature BMDCs (2×10 <sup>6</sup> cells mL <sup>-1</sup> ) were incubated with FOL-M@NLP (2×10 <sup>7</sup> CFU     |
|-----|---|
| 200 | mL <sup>-1</sup> ) or other groups for 24 h. Final concentration of NLP was 50 μg mL <sup>-1</sup> . The LPS        |
| 201 | concentration was 2.5 µg mL <sup>-1</sup> . After 24 h, activated DCs were detected via flow                        |
| 202 | cytometry (CD11c+CD80+CD86+). DCs matured by antigen stimulation were   |
| 203 | cocultured with lymphocytes from the mouse spleen at a ratio of 1:10. On day 2, the                                 |
| 204 | CD8 <sup>+</sup> CD69 <sup>+</sup> and CD8 <sup>+</sup> CD25 <sup>+</sup> T cells were detected via flow cytometry. |
| 205 |   |
| 206 | 2.8. In vivo biodistribution  |
| 207 | FOL-M@NLP was stained with DiR and subcutaneously injected in the left abdomen                                      |
| 208 | of mice bearing 4T1-NY-ESO-1 subcutaneous tumour. At predetermined time points,                                     |
| 209 | mice were scanned and images were captured by CRi Maestro In Vivo Imaging System                                    |
| 210 | (Cambridge Research & Instrumentation, USA). Afterwards, mice were sacrificed, and                                  |
| 211 | tumours, bilateral tumor-draining lymph nodes (TDLNs) and major organs were   |
| 212 | harvested for imaging ex vivo.  |
| 213 |   |
| 214 | 2.9. Construction of tumour models and therapy  |
| 215 | The primary B16F10-NY-ESO-1 melanoma mouse model was established via the  |
| 216 | subcutaneous injection of 5×10 <sup>5</sup> B16F10-NY-ESO-1 cells into C57BL/6J mice. These                         |
| 217 | mice were randomly divided into 7 groups ( $n=5$ ), which were injected with normal                                 |
| 218 | saline (NS); NLP; FOLactis; FOL-M; a physical mixture of aluminum hydroxide gels                                    |
| 219 | adjuvant (Biodragon, China) and three peptides, abbreviated as Al(OH)3+NLP; FOL-                                    |
| 220 | M+NLP and FOL-M@NLP subcutaneously on days 3, 6, 9, and 14 following tumour   |

| 221 | inoculation. The dosage was that 5×10 <sup>8</sup> CFU of FOLactis per mouse and 100 μg of each |
|-----|---|
| 222 | peptide per mouse. The dosage of the classic adjuvant aluminum hydroxide was 60 µg              |
| 223 | per mouse. During the treatment, tumour volume and body weight of each mouse was                |
| 224 | recorded every 2 days. On day 17, mice from all groups were sacrificed. TDLNs and               |
| 225 | tumours were obtained from the mice in each group for immune efficacy testing.                  |
| 226 | The B16F10-NY-ESO-1 melanoma lung metastasis mouse model was constructed via                    |
| 227 | the injection of 5×10 <sup>5</sup> B16F10-NY-ESO-1 cells into the tail vein of C57BL/6J mice.   |
| 228 | These mice were randomly divided into 6 groups (n=5), namely NS group, NLP group,               |
| 229 | FOLactis group, FOL-M group, FOL-M+NLP group and FOL-M@NLP group. On                            |
| 230 | days 3, 6, 9 and 16 following tumour inoculation, each group of mice received                   |
| 231 | subcutaneous administration of the same dose as described above. During the treatment,          |
| 232 | body weight of each mouse was recorded every 2 days. On day 20, mice from all groups            |
| 233 | were sacrificed. TDLNs, spleens and lungs with metastases were obtained from the                |
| 234 | mice in each group for immune efficacy testing.   |
| 235 | To establish postoperative recurrence-preventing models, 5×10 <sup>5</sup> 4T1-NY-ESO-1 cells   |
| 236 | were inoculated subcutaneously into BALB/c mice, and the mice were then randomly                |
| 237 | divided into 6 groups ( $n=5$ ). One week after tumour inoculation, the average                 |
| 238 | subcutaneous tumour volume of each group was 95-100 mm³, and the tumour-bearing                 |
| 239 | mice underwent subtotal tumour resection under general anaesthesia. Approximately 5             |
| 240 | mm <sup>3</sup> of tumour remained after surgery. 6 groups of postoperative mice were           |
| 241 | subcutaneously injected with NS, NLP, FOLactis, FOL-M, FOL-M+NLP, or FOL-                       |
| 242 | M@NLP on postoperative days 3, 6, 9, and 16, respectively. Each group of mice                   |

#### Journal Pre-proof

| 243   | received administration of the same dose as described above. The mice were monitored  |
|---|---|
| 244   | every 2 days postoperatively for tumour volume, body weight, and survival, and the  |
| 245   | survival endpoint was set when the tumour volume reached 1500 mm <sup>3</sup> . On  |
| 246   | postoperative day 90, rechallenge experiments were performed via the subcutaneous   |
| 247   | inoculation of 5×10 <sup>5</sup> 4T1-NY-ESO-1 cells in the surviving mice and 3 BALB/c mice   |
| 248   | without a history of tumour bearing, and the tumour volume, vitality, health status and   |
| 249   | survival of the mice were observed.   |
| 250   | To explore the preventive potency of the biovaccine, BALB/c mice were randomly  |
| 251   | divided into 3 groups and subcutaneously injected with NS, NLP and FOL-M@NLP on   |
| 252   | days 1, 4, 7 and 14. On day 19, 5×10 <sup>5</sup> 4T1-NY-ESO-1 cells were inoculated  |
| 253   | subcutaneously into the mice and the mice were monitored every 2 days for tumour  |
|   |   |
| 254   | volume and body weight.   |
| 254<br>255  | volume and body weight.   |
|   | volume and body weight.  2.10. Flow cytometry   |
| 255   |   |
| 255<br>256  | 2.10. Flow cytometry  |
| <ul><li>255</li><li>256</li><li>257</li></ul>                         | 2.10. Flow cytometry  Anti-mouse CD11c-FITC (117306), anti-mouse CD80-APC (104714), anti-mouse  |
| <ul><li>255</li><li>256</li><li>257</li><li>258</li></ul>             | 2.10. Flow cytometry  Anti-mouse CD11c-FITC (117306), anti-mouse CD80-APC (104714), anti-mouse CD86-PE (105008), anti-mouse CD8a-PerCP/Cyanine5.5 (100734), anti-mouse CD4-   |
| <ul><li>255</li><li>256</li><li>257</li><li>258</li><li>259</li></ul> | 2.10. Flow cytometry  Anti-mouse CD11c-FITC (117306), anti-mouse CD80-APC (104714), anti-mouse CD86-PE (105008), anti-mouse CD8a-PerCP/Cyanine5.5 (100734), anti-mouse CD4-PE (100408), anti-mouse CD69-FITC (104506), anti-mouse CD25-APC (101910),  |
| 255<br>256<br>257<br>258<br>259<br>260                                | 2.10. Flow cytometry  Anti-mouse CD11c-FITC (117306), anti-mouse CD80-APC (104714), anti-mouse CD86-PE (105008), anti-mouse CD8a-PerCP/Cyanine5.5 (100734), anti-mouse CD4-PE (100408), anti-mouse CD69-FITC (104506), anti-mouse CD25-APC (101910), anti-mouse H-2Kb/H-2Db- PerCP/Cyanine5.5 (114620), anti-mouse I-A/I-E-PE   |
| 255<br>256<br>257<br>258<br>259<br>260<br>261                         | 2.10. Flow cytometry  Anti-mouse CD11c-FITC (117306), anti-mouse CD80-APC (104714), anti-mouse CD86-PE (105008), anti-mouse CD8a-PerCP/Cyanine5.5 (100734), anti-mouse CD4-PE (100408), anti-mouse CD69-FITC (104506), anti-mouse CD25-APC (101910), anti-mouse H-2Kb/H-2Db- PerCP/Cyanine5.5 (114620), anti-mouse I-A/I-E-PE (107608), anti-mouse CD86-PE/Cyanine7 (105014), anti-mouse CD8a-APC |

| 265 | CD44-PE (103008), anti-mouse CD62L-PE/Cyanine7 (104418), anti-mouse FOXp3-                    |
|-----|---|
| 266 | PE (126404), anti-mouse NK1.1-PE (156504), anti-mouse CD11b-FITC (101206),                    |
| 267 | anti-mouse F4/80-PE/Cyanine7 (123114), and anti-mouse CD206-APC (141708)                      |
| 268 | antibodies were purchased from Biolegend (USA). Anti-mouse CD80-BV421 (562611)                |
| 269 | and anti-mouse CD103-BV605 (748257) were purchased from BD (USA).                             |
| 270 | TDLNs, spleens and tumour tissues were harvested from the mice for further analysis.          |
| 271 | Single-cell suspensions from TDLNs and spleens were prepared via the mechanical               |
| 272 | lapping method. The tumour tissues were cut into pieces and then digested with                |
| 273 | collagenase type IV (1 mg mL <sup>-1</sup> , Sigma-Aldrich, USA) for 2 h at 37°C. All samples |
| 274 | were resuspended in ice-cold normal saline, stained with specific antibodies for 30 min       |
| 275 | at 4°C in the dark, and washed before analysis. For molecules expressed intracellularly,      |
| 276 | such as FOXp3, a Cytofix/Cytoperm™ Fixation/Permeabilization Kit (554714, BD,                 |
| 277 | USA) was used for the fixation and permeabilization of the cells. The cells were              |
| 278 | detected using CytoFLEX (Beckman, USA) and analysed by FlowJo or NovoExpress                  |
| 279 | software.   |
| 280 |   |
| 281 | 2.11. Cytokine measurement  |
| 282 | Tumours from each treatment group were collected, weighed, and then rapidly frozen            |
| 283 | in liquid nitrogen. Subsequently, the tumour samples were lysed in RIPA buffer                |
| 284 | (Beyotime, China) containing 1% protease and phosphatase inhibitor cocktail (NCM              |
| 285 | Biotech, China) on ice for 30 min, with approximately 100 mg of samples lysed in 1            |
| 286 | mL of buffer, followed by centrifugation (12000 ×g, 10 min, 4°C). The protein                 |

| 287 | concentration of the supernatant was standardized to 4 $\mu g$ $\mu L^{-1}$ after determined by   |
|-----|---|
| 288 | bicinchoninic acid assay. Then, 25 $\mu L$ of samples (100 $\mu g$ total protein per sample) were |
| 289 | analysed using LEGENDplex <sup>TM</sup> MU Th1/Th2 Panel (8-plex) w/ VbP V03 (Biolegend,          |
| 290 | USA) and the cytokines in TME were detected by flow cytometry. Additionally, 25 $\mu L$           |
| 291 | of serum from each mouse in treatment groups were harvested and analysed using                    |
| 292 | LEGENDplex™ MU Th1/Th2 Panel (8-plex) w/ VbP V03, and the cytokines in serum                      |
| 293 | were detected by flow cytometry.  |
| 294 |   |
| 295 | 2.12. RNA sequencing and gene expression analysis of the tumour metastasis niche                  |
| 296 | Metastases from NS group and FOL-M@NLP (FMN) group were rapidly frozen in                         |
| 297 | liquid nitrogen after collection. The mRNA samples from the two groups were                       |
| 298 | subjected to RNA-seq (BerryGenomics, China). Mus_musculus-NCBI-GRCm39 was                         |
| 299 | selected as the reference genome. The sequencing data were statistically analysed via             |
| 300 | RStudio. Volcano plots, heatmaps and bubble plots for Kyoto Encyclopedia of Genes                 |
| 301 | and Genomes (KEGG) enrichment and Gene Ontology (GO) enrichment analyses were                     |
| 302 | generated. Cytoscape was used to perform protein-protein interaction (PPI) analysis               |
| 303 | and screen for hub genes.   |
| 304 |   |
| 305 | 2.13. Specific immune response detection  |
| 306 | BALB/c mice were received various stimulations on days 1, 4, 7, and 14. The doses                 |
| 307 | were the same as described in section 2.9. One week after the final injection, the spleens        |
| 308 | were harvested, and lymphocytes were isolated as effector cells. The effector cells were          |

| 309 | co-incubated with 4T1-NY-ESO-1 cells and specific IFN- $\gamma$ secreted by effector cells          |
|-----|---|
| 310 | were detected by ELISPOT. For determination of the destructive capacity of effector                 |
| 311 | cells on target cells, 4T1-NY-ESO-1 and wild-type 4T1 cells served as target cells,                 |
| 312 | which were adjusted to $1\times10^6$ cells mL <sup>-1</sup> and labelled with CFSE (Abcam Plc, UK). |
| 313 | Target cells were cocultured with effector cells for 6 h at a ratio of 1:10 and then labelled       |
| 314 | with propidium iodide (PI, 100 ng mL <sup>-1</sup> , Merck, Germany). The cells were incubated      |
| 315 | in the dark at room temperature for 10 min, and PI+ target cells were detected by flow              |
| 316 | cytometry and analysed using NovoExpress software.  |
| 317 |   |
| 318 | 2.14. Statistical analysis  |
| 319 | Statistical analyses were performed via GraphPad Prism 9.5.1 software. All the data are             |
| 320 | presented as the means $\pm$ SD of at least three independent experiments. $P$ values were          |
| 321 | calculated via two-tailed unpaired Student's t tests, one-way ANOVA or two-way                      |
| 322 | ANOVA. The log-rank (Mantel-Cox) test was used for survival analysis. Flow                          |
| 323 | cytometry data were analysed via FlowJo 10.8.1 and NovoExpress.                                     |
| 324 |   |
| 325 | 3. Results  |
| 326 | 3.1. NY-ESO-1 sequence analysis and epitope prediction  |
| 327 | Bioinformatic methods were used to screen long peptides with multiple epitopes from                 |
| 328 | NY-ESO-1. On the basis of a comprehensive survey of HLA I and II restrictive loci,                  |
| 329 | which includes 812211 unrelated volunteers from diverse regions of China, 6 HLA-A                   |
| 330 | alleles were selected that cover 66.26% of the HLA-A alleles of Chinese people: HLA-                |

A\*01:01 (3.59%), HLA-A\*02:01 (12.04%), HLA-A\*02:01 (20.89%), HLA-A\*24:02 331 (15.55%), HLA-A\*30:01 (5.97%) and HLA-A\*33:03 (8.23%) [14]. Moreover, 8 HLA-332 333 DRB1 alleles were also filtered according to the survey and accounted for 66.6% of the HLA-DRB1 alleles identified in Chinese people. These 8 alleles were HLA-334 DRB1\*03:01 (5.1%), HLA-DRB1\*04:05 (4.82%), HLA-DRB1\*07:01 (9.66%), HLA-335 DRB1\*08:03 (6.31%), HLA-DRB1\*09:01 (14.79%), HLA-DRB1\*11:01 (5.63%), 336 HLA-DRB1\*12:02 (8.71%), and HLA-DRB1\*15:01 (11.58%) [14]. On the basis of the 337 screening results, 3 long peptides derived from the NY-ESO-1 sequence were identified. 338 339 NLP-184-111: ESRLLEFYLAMPFATPMEAELARRSLAQ; NLP-2<sub>122-153</sub>: LLKEFTVSGNILTIRLTAADHRQLQLSISSCL; 340 NLP-3<sub>157-180</sub>: SLLMWITQCFLPVFLAQPPSGQRR. These 3 peptides contained multiple epitopes 341 342 that have high affinity for major HLA-I and HLA-II molecules (Table 1). The 3 peptides also contained epitopes with affinity for MHC molecules in BALB/c mice and 343 C57BL/6J mice (Tables 2 and 3), and the binding affinity to MHC molecules of the 344 345 selected peptides has been validated by ELISPOT (Fig. 1A). Therefore, these 2 model organisms were selected in this study to investigate the tumour suppressor effects of 346 these peptides. 347

348

**Table 1** Potential epitopes for different MHC molecules in the NY-ESO-1 sequence

|          |             | CD8 <sup>+</sup> T-cell epitope | e           |          | CD4 <sup>+</sup> T-cell epitope |             |
|----------|-------------|---------------------------------|-------------|----------|---------------------------------|-------------|
| Peptides | Position    | Sequence                        | HLA-I       | Position | Sequence                        | HLA-II      |
|          | <b>//01</b> | = -1                            | restriction |          |                                 | restriction |

| NLP-1: ESRLLEFYLAMPFATPMEAELARRSLAQ |   |                |         |         |                  |            |  |  |
|-------------------------------------|---|----------------|---------|---------|------------------|------------|--|--|
|                                     | 84-91                                   | ESRLLEFY       | A*01:01 | 84-97   | ESRLLEFYLAMPFA   | DRB1*15:01 |  |  |
|                                     | 86-94                                   | RLLEFYLAM      | A*02:01 |         |                  |            |  |  |
|                                     | 97-106                                  | ATPMEAELAR     | A*11:01 |         |                  |            |  |  |
|                                     | 97-106                                  | ATPMEAELAR     | A*33:03 |         |                  |            |  |  |
| NLP-2: L                            | NLP-2: LLKEFTVSGNILTIRLTAADHRQLQLSISSCL |                |         |         |                  |            |  |  |
|                                     | 127-135                                 | TVSGNILTI      | A*02:01 | 123-136 | LKEFTVSGNILTIR   | DRB1*09:01 |  |  |
|                                     | 127-136                                 | TVSGNILTIR     | A*11:01 | 124-137 | KEFTVSGNILTIRL   | DRB1*07:01 |  |  |
|                                     | 127-136                                 | TVSGNILTIR     | A*33:03 | 128-143 | VSGNILTIRLTAADHR | DRB1*12:02 |  |  |
|                                     | 139-147                                 | AADHRQLQL      | A*01:01 | 129-144 | SGNILTIRLTAADHRQ | DRB1*08:03 |  |  |
|                                     |   |                |         | 135-148 | IRLTAADHRQLQLS   | DRB1*03:01 |  |  |
| NLP-3: S                            | LLMWITQ                                 | CFLPVFLAQPPSGQ | RR      |         |                  |            |  |  |
|                                     | 157-165                                 | SLLMWITQC      | A*02:01 | 166-180 | FLPVFLAQPPSGQRR  | DRB1*04:05 |  |  |
|                                     | 160-170                                 | MWITQCFLPVF    | A*24:02 | 167-180 | LPVFLAQPPSGQRR   | DRB1*11:01 |  |  |
|                                     | 171-179                                 | LAQPPSGQR      | A*11:01 |         |                  |            |  |  |
|                                     | 171-180                                 | LAQPPSGQRR     | A*33:03 |         |                  |            |  |  |

351

# Table 2 Potential epitopes for different MHC molecules of BALB/c mice contained in

## 352 NLP

|          |          | CD8 <sup>+</sup> T-cell epitop | oe          |          | CD4 <sup>+</sup> T-cell epitope |             |
|----------|----------|--------------------------------|-------------|----------|---------------------------------|-------------|
| Peptides | D '.'    | G                              | Н-2 І       | D ''     | G.                              | H-2 II      |
|          | Position | Sequence                       | restriction | Position | Sequence                        | restriction |

NLP-1: ESRLLEFYLAMPFATPMEAELARRSLAQ

| 90-100            | FYLAMPFATPM      | H-2-K <sup>d</sup> | 94-107  | MPFATPMEAELARR  | H2-IA <sup>d</sup> |
|-------------------|------------------|--------------------|---------|-----------------|--------------------|
| 94-104            | MPFATPMEAEL      | H-2-L <sup>d</sup> |         |                 |                    |
| 97-104            | ATPMEAEL         | H-2-D <sup>d</sup> |         |                 |                    |
| NLP-2: LLKEFTVSGI | NILTIRLTAADHRQLO | QLSISSCL           |         |                 |                    |
| 127-135           | TVSGNILTI        | H-2-K <sup>d</sup> | 129-143 | SGNILTIRLTAADHR | H2-IA <sup>d</sup> |
| 129-137           | SGNILTIRL        | H-2-L <sup>d</sup> | 132-146 | ILTIRLTAADHRQLQ | H2-IE <sup>d</sup> |
| 139-147           | AADHRQLQL        | H-2-D <sup>d</sup> |         |                 |                    |
| NLP-3: SLLMWITQC  | FLPVFLAQPPSGQRF  | 8                  |         | ?               |                    |
| 163-171           | TQCFLPVFL        | H-2-K <sup>d</sup> | 167-180 | LPVFLAQPPSGQRR  | H2-IE <sup>d</sup> |

353

354

## Table 3 Potential epitopes for different MHC molecules of C57BL/6J mice contained

168-178

H2-IA<sup>d</sup>

PVFLAQPPSGQ

## 355 in NLP

|           |           | CD8 <sup>+</sup> T-cell epitope | e                  |          | CD4 <sup>+</sup> T-cell epitope |                    |
|-----------|-----------|---------------------------------|--------------------|----------|---------------------------------|--------------------|
| Peptides  | Position  | Sequence                        | Н-2 І              |          | Sequence                        | H-2 II             |
|           |           |                                 | restriction        | Position |                                 | restriction        |
| NLP-1: ES | SRLLEFYLA | MPFATPMEAELA                    | RRSLAQ             |          |                                 |                    |
|           | 86-94     | RLLEFYLAM                       | H-2-K <sup>b</sup> | 93-106   | AMPFATPMEAELAR                  | H2-IA <sup>b</sup> |
|           | 96-104    | FATPMEAEL                       | H-2-D <sup>b</sup> |          |                                 |                    |

NLP-2: LLKEFTVSGNILTIRLTAADHRQLQLSISSCL

127-135 TVSGNILTI H-2-D<sup>b</sup>

|          | 138-145   | TAADHRQL      | H-2-K <sup>b</sup> |         |             |                    |
|----------|-----------|---------------|--------------------|---------|-------------|--------------------|
| NLP-3: S | LLMWITQCF | LPVFLAQPPSGQR | R.R.               |         |             |                    |
|          | 162-170   | ITQCFLPVF     | H-2-K <sup>b</sup> | 168-178 | PVFLAQPPSGQ | H2-IA <sup>b</sup> |
|          | 163-171   | TQCFLPVFL     | H-2-D <sup>b</sup> |         |             |                    |

357

358

359

360

361

362

363

364

365

366

367

368

369

370

371

372

373

3.2. Preparation and characterization of FOL-M@NLP and cell lines

2-Methylimidazole binds to Mg<sup>2+</sup> via coordination to form MOFs for loading NLP [17-19]. Under the action of electrostatic force and imine bonding, MOFs that load peptides can spontaneously attach to the surface of FOLactis to construct FOL-M@NLP [20, 21]. Images captured by scanning electron microscopy (SEM) revealed that FOLactis and FOL-M@NLP were ellipsoidal, the surface of FOLactis was smooth, whereas granular MOF attached to the rough surface of FOL-M@NLP (Fig. 1B and S1). The distribution of elements on the surface of the biovaccine was detected by chemical mapping using energy dispersive spectroscopy (EDS) in SEM, and the proportions of various elements were measured. (Fig. 1C and 1D). Through dynamic light scattering (DLS) analysis, the sizes of FOLactis and FOL-M@NLP were evenly distributed, and the particle size of FOL-M@NLP (1353  $\pm$  147.4 nm) was larger than that of FOLactis  $(1050 \pm 23.25 \text{ nm})$  (Fig. 1E and 1F). There was no significant difference in the polydispersity index (PDI) between the two particles (Fig. 1G). Due to teichoic acid and peptidoglycan in the cell wall, the surface of FOLactis was negatively charged with a zeta potential of  $-25.50 \pm 0.36$  mV. After loading of MOF containing NLP, the zeta potential was elevated to  $-17.23 \pm 0.15$  mV (Fig. 1H). The encapsulation efficiencies

| (EE) of 3 selected peptides in the biovaccines were determined via high-performance     |
|---|
| liquid chromatography and are depicted in Fig. 11. The EE of NLP-1 was approximately    |
| 55% regardless of input dosage, while the EE of NLP-2 increased with more feeding       |
| peptides. NLP-3 exhibited ideal binding capacity during preparation, with EE reaching   |
| above 90%. Under the simulated acidic immune microenvironment, most of the 3            |
| peptides would be released from the biovaccine within 48 h (Fig. 1J). After co-cultured |
| with splenocytes in the cell culture medium for 24 h and activated for 16 h, FOLactis   |
| from the biovaccine rapidly enter the logarithmic growth phase in the GM17 medium       |
| containing chloramphenicol and reach the plateau phase in about 10 h (Fig. 1K). While   |
| coated on GM17 agar plates containing chloramphenicol and incubated at 30°C,            |
| FOLactis from the biovaccine formed monoclonal colonies, indicates that the activity    |
| of FOLactis itself was not obviously affected after being loaded with MOF (Fig. 1L      |
| and S2).  |
| 4T1 breast cancer cells and B16F10 melanoma cells were selected for the construction    |
| of tumour models. The CTAG1B gene was integrated into the DNA of these host cells       |
| via lentiviral infection, and the expression of NY-ESO-1 in 4T1-NY-ESO-1 cells and      |
| B16F10-NY-ESO-1 cells was verified by Western blotting and immunohistochemistry         |
| (Fig. S3).  |

393 3.3. In vitro immune response induced by FOL-M@NLP

We coincubated FOL-M+NLP and FOL-M@NLP with BMDCs at different bacterial concentrations. As shown in **Fig. 2A**, the engineered bacteria loaded with NLP did not

show obvious cytotoxicity. 396 To explore the ability of FOL-M@NLP to be taken up by BMDCs in vitro, immature 397 BMDCs were coincubated with NLP-3-Cy5 and FOL-M@NLP-3-Cy5. Then, the 398 BMDCs were collected at different time points during coincubation (0.5 h, 2 h, 6 h, 12 399 h, 24 h, 36 h, and 48 h) for flow cytometry analysis (Fig. 2B and S4). Compared with 400 NLP-3-Cy5, FOL-M@NLP-3-Cy5 could be taken up by BMDCs continuously and 401 efficiently. The uptake and intracellular distribution of Cy5 by DCs were analysed via 402 confocal microscopy. Compared with NLP-3-Cy5, FOL-M@NLP-3-Cy5 accumulated 403 404 more in the cytoplasm of BMDCs (Fig. 2C). To explore the ability of FOL-M@NLP to stimulate BMDC maturation in vitro, we 405 cocultured immature BMDCs with 1640 medium containing different substances, and 406 407 the levels of the costimulatory molecules CD80 and CD86 on the surface of BMDCs (CD11c<sup>+</sup>) were detected via flow cytometry. After stimulation with FOL-M@NLP-1, 408 FOL-M@NLP-2, and FOL-M@NLP-3, the proportions of mature DCs reached 63.23 409 410  $\pm 1.68\%$ , 63.23  $\pm 2.03\%$ , and 62.33  $\pm 1.52\%$ , respectively. The proportions in the NLP-1, NLP-2, and NLP-3 groups were  $47.05 \pm 1.11\%$ ,  $45.98 \pm 3.54\%$ , and  $32.48 \pm 0.25\%$ , 411 respectively. After stimulation with lipopolysaccharide (LPS), the proportion of mature 412 413 DCs reached  $57.25 \pm 2.03\%$  (Fig. 2D and S5). It can be concluded that the biovaccines (FOL-M@NLP-1, FOL-M@NLP-2, and FOL-M@NLP-3) promoted the maturation of 414 BMDCs for the proportion of mature DCs in each of the 3 groups was greater than 60%, 415 416 and the maturation-promoting effect of FOL-M@NLP was significantly better than that of the naked peptides (NLP-1, NLP-2, and NLP-3). 417

| 418 | To explore the activation of T cells by this biovaccine, immature BMDCs were   |
|-----|--|
| 419 | incubated with 1640 medium containing different components and then cocultured with  |
| 420 | lymphocytes. On the next day, the proportions of CD8 <sup>+</sup> CD69 <sup>+</sup> T cells and CD8 <sup>+</sup> CD25 <sup>+</sup> |
| 421 | T cells in the FOL-M@NLP group were significantly greater than that in the NLP and   |
| 422 | the FOLactis groups, with the FOL-M@NLP group proportionally reaching 45.80 $\pm$  |
| 423 | 0.51% and 20.34 $\pm$ 0.50%, respectively (Fig. 2E, 2F and S6), which revealed that FOL-   |
| 424 | M@NLP was able to induce T-cell activation better than the naked peptides.   |
| 425 |  |
| 426 | 3.4. Biodistribution and antitumour effect of FOL-M@NLP, and immune response   |
| 427 | induced by FOL-M@NLP in vivo   |
| 428 | Firstly, to investigate the biodistribution of FOL-M@NLP, the biovaccine was labeled   |
| 429 | with DiR and administered subcutaneously. The biovaccine exhibited in vivo   |
| 430 | persistence for approximately 2 weeks (Fig. 3A and 3C). Upon administration, the   |
| 431 | biovaccine rapidly accumulated within the local tumor-draining lymph node (TDLN)   |
| 432 | and the tumour site, reaching peak enrichment within 24 hours for sustained therapeutic  |
| 433 | action (Fig. 3B, 3D and 3E). Notably, no obvious signal was detected in other organs,  |
| 434 | suggesting the favorable biosafety profile of the biovaccine.  |
| 435 | Next, the antitumour effect of FOL-M@NLP in vivo was assessed. A subcutaneous  |
| 436 | B16F10-NY-ESO-1 melanoma mouse model was constructed and different treatments  |
| 437 | was administered (Fig. 3F). As depicted in Fig. 3G and S7, the application of FOL-   |
| 438 | M@NLP significantly limited the growth of melanoma, while compared with NLP and  |
| 439 | FOLactis alone. No statistically significant differences were found among the body   |

weights of the 7 groups of mice at each time point (Fig. 3H). Tumours were harvested 440 at the observation endpoint, the size and the average weight of the tumours from the 441 FOL-M@NLP group were the lowest, indicating the potent antitumour effect of the 442 biovaccine (Fig. 3I and 3J). 443 To determine the mechanism of the immunological responses induced by FOL-444 M@NLP in vivo, Tumours and TDLNs were harvested from the mice in all the groups 445 to detect changes in the immune microenvironment via flow cytometry. In TDLNs, 446 FOL-M@NLP could increase the level of MHC I  $(8.57 \times 10^3 \pm 1.55 \times 10^3)$  and MHC II 447  $(10.13 \times 10^2 \pm 1.17 \times 10^2)$  expression on DCs for antigen presentation (Fig. 4A, 4B and 448 **S8).** In TME, the proportion of CD103<sup>+</sup> DCs in the FOL-M@NLP group (42.04  $\pm$ 449 16.23%) was highest and had a nearly 18-fold increase compared to the NS group (2.39 450 ± 1.11%), and the ratio of CD8<sup>+</sup> DCs showed a 5.2-fold increase in the FOL-M@NLP 451 group (19.97  $\pm$  9.49%), which was higher than the Al(OH)<sub>3</sub>+NLP group (9.64  $\pm$ 452 7.17%) (Fig. 4C, 4D and S9). In TME, the expressions of MHC I  $(4.52 \times 10^4 \pm 0.60 \times 10^4)$ 453  $10^4$ ) and MHC II  $(6.00 \times 10^3 \pm 0.82 \times 10^3)$  were also the highest while compared with 454 other groups, indicating antigen presentation might be further facilitated (Fig. 4E, 4F, 455 **4K and 4L**). In the MHC I<sup>+</sup> DCs, the proportion of mature DCs (CD80<sup>+</sup>CD86<sup>+</sup>) in the 456 FOL-M@NLP group (30.44 ± 16.65%) was significantly higher while compared with 457 the NS group (2.02  $\pm$  1.09%), the NLP group (2.59  $\pm$  0.33%), the FOLactis group 458  $(5.67 \pm 4.05\%)$  and the FOL-M group  $(3.51 \pm 1.17\%)$ . The peptide-major 459 histocompatibility complex (pMHC) on these DCs might be recognized by the receptor 460 of CD8<sup>+</sup> T cells (Fig. 4G and S10A). Similarly, FOL-M@NLP promoted the 461

| maturation of MHC II <sup>+</sup> DCs (35.73 ± 19.37%) more sufficiently than Al(OH) <sub>3</sub> +NLP |
|--|
| group (14.74 $\pm$ 4.47%) and other groups, with CD4 $^+$ T cells more activated (Fig. 4H              |
| and S10B). In the presence of cytokines, the activated CD8 <sup>+</sup> T cells express IFN-γ to       |
| exert specific cytotoxicity and granzyme B to induce apoptosis of tumour cells. The                    |
| biovaccine FOL-M@NLP had successfully enhanced the production of IFN- $\gamma$ (29.70 $\pm$            |
| 2.21%) and granzyme B (19.14 $\pm$ 6.86%) in the cytoplasm of CD8 <sup>+</sup> T cells (Fig. 4I,       |
| 4J and S11). Relevant cytokines in TME had also be tested to analyse the changes of                    |
| cytokine levels within the TME. With the application of FOL-M@NLP, the level of IL-                    |
| 4, IL-6, IL-10 and IL-13 in TME had decreased (Fig. S12). No Significant differences                   |
| in the levels of various cytokines in the serum have been found, indicate no risk of                   |
| severe systemic inflammatory response following application of the biovaccine, and                     |
| elucidate the safety profile of this biovaccine (Fig. S13).  |

3.5. Anti-metastatic effect of FOL-M@NLP, and immune response induced by FOL-

477 M@NLP in a melanoma metastasis model

To estimate the anti-metastatic effect of FOL-M@NLP in vivo, a B16F10-NY-ESO-1 melanoma lung metastasis mouse model was constructed. Model construction, treatment planning, and observation endpoint are shown in Fig. 5A. Throughout the treatment period, changes in the body weights of the mice were observed, and there was no significant difference among the groups (Fig. 5B). The weights of lungs with

metastases were measured at observation endpoint, and the average weight of the FOL-

| 484 | M@NLP group was the lowest, indicating that the fewest metastases were attached to                                |
|-----|---|
| 485 | the lungs (Fig. 5C). Many black metastases were attached to the lungs in the NS,                                  |
| 486 | FOLactis and FOL-M groups, and the pulmonary tissue structure was completely                                      |
| 487 | destroyed, whereas fewer metastases were observed in the NLP and FOL-M+NLP  |
| 488 | groups. The metastases of the FOL-M@NLP group were the fewest (Fig. 5D).  |
| 489 | Hematoxylin-eosin staining images of the lungs revealed that the lung tissue structures                           |
| 490 | of the FOL-M@NLP group were clear and that the alveolar structures were intact, with                              |
| 491 | thin and uniform alveolar walls and no many abnormal cells in the alveolar cavity;                                |
| 492 | moreover, the bronchial mucosal epithelium was intact. In the other groups, multiple                              |
| 493 | focal hyperchromatic areas were visible and distributed within the pulmonary                                      |
| 494 | parenchyma. The metastatic foci presented as nodules or showed diffuse infiltration.                              |
| 495 | The surrounding lung tissue was compressed, and the local alveolar structures collapsed                           |
| 496 | or disappeared. Larger metastatic foci coalesced into patches (Fig. 5E).  |
| 497 | To determine the mechanism of the immunological responses induced by FOL-   |
| 498 | M@NLP, lungs with metastases, spleens and TDLNs from each group were harvested                                    |
| 499 | from the mice in all the groups to detect changes in the immune microenvironment via                              |
| 500 | flow cytometry. In TDLNs, the proportion of CD8 <sup>+</sup> T <sub>EM</sub> cells in the FOL-M@NLP               |
| 501 | group (27.12 $\pm$ 2.07%) was significantly greater than that in the other groups, indicating                     |
| 502 | that, compared with those in the other controls, naive CD8 <sup>+</sup> T cells were more inclined                |
| 503 | to differentiate into CD8 <sup>+</sup> T <sub>EM</sub> cells that can destroy target cells after being stimulated |
| 504 | with FOL-M@NLP (Fig. 6A and S14A). The proportion of CD4 <sup>+</sup> T <sub>EM</sub> cells in the FOL-           |
| 505 | M@NLP group $(37.66 \pm 3.09\%)$ was also significantly greater than that in the other                            |

| 506 | groups, indicating that the cell population capable of exerting antitumour immune                        |
|-----|--|
| 507 | effects in TDLNs was further expanded (Fig. 6B and S14B).  |
| 508 | Compared with the NS group (5.60 $\pm$ 0.45%), both the FOL-M+NLP (8.46 $\pm$ 1.25%)                     |
| 509 | and FOL-M@NLP (9.14 $\pm$ 0.91%) groups promoted the proliferation of cytotoxic CD8+                     |
| 510 | T cells in the spleen, and the promotion of FOL-M@NLP was more obvious than that                         |
| 511 | of the NLP group (7.00 $\pm$ 0.82%) (Fig. 6C and S15A). Similar to TDLNs, in spleen,                     |
| 512 | the proportion of CD8 <sup>+</sup> $T_{EM}$ cells in the FOL-M@NLP group (18.56 $\pm$ 1.56%) was         |
| 513 | significantly greater than that in the other groups (Fig. 6D and S15B). The proportion                   |
| 514 | of CD4 $^+$ T <sub>EM</sub> cells in the FOL-M@NLP group (24.94 $\pm$ 2.31%) was also the highest        |
| 515 | and was significantly different from that in the other groups except for the FOL-M                       |
| 516 | group (24.50 $\pm$ 2.09%) (Fig. 6E and S15C). Compared with other controls, the                          |
| 517 | biovaccine can fully mobilize the immune response potential of the spleen.                               |
| 518 | In the tumour metastasis niche, the FOL-M@NLP group had the highest proportion of                        |
| 519 | CD8 <sup>+</sup> $T_{EM}$ cells (19.86 $\pm$ 4.79%) in all groups (Fig. 6F and S16A). In the presence of |
| 520 | different cytokines, helper T cells can differentiate into subpopulations such as Th1                    |
| 521 | cells, Th2 cells and regulatory T cells (Tregs). Tregs accounted for the lowest proportion               |
| 522 | of helper T cells in the FOL-M@NLP group (3.23 $\pm$ 0.56%) among all groups,                            |
| 523 | suggesting that Treg proliferation and infiltration were significantly limited in the                    |
| 524 | presence of the biovaccine (Fig. 6G and S16B). The FOL-M@NLP vaccine also                                |
| 525 | activated innate immunity in the tumour metastasis niche. The degree of NK cell                          |
| 526 | infiltration was greater in both the FOL-M+NLP group (5.48 $\pm$ 2.04%) and the FOL-                     |
| 527 | M@NLP group (5.57 $\pm$ 1.47%) than in the NS group (2.93 $\pm$ 0.29%) (Fig. 6H and                      |

| 528 | S16C). After vaccine stimulation, the direction of macrophage polarization changed                          |
|-----|---|
| 529 | after activation. The ratio of classically activated macrophages/alternatively activated                    |
| 530 | macrophages was greater in the FOL-M+NLP group (0.48 $\pm$ 0.10) than in the NS group                       |
| 531 | $(0.19 \pm 0.07)$ and the NLP group $(0.24 \pm 0.09)$ , whereas the ratio in the FOL-M@NLP                  |
| 532 | group $(0.74 \pm 0.17)$ was significantly greater than the ratios in all the other groups (Fig.             |
| 533 | 61). Compared with those in the other groups, the macrophages in the FOL-M@NLP                              |
| 534 | group were more inclined to differentiate towards the classically activated type (17.93                     |
| 535 | $\pm 6.66\%$ ) (Fig. S17).  |
| 536 | Immunofluorescence staining of lungs with metastases revealed that the IFN- $\gamma^+$ cells in             |
| 537 | the FOL-M@NLP group were mainly clustered in some fields and were well infiltrated                          |
| 538 | there, whereas the IFN- $\gamma^+$ cells in the other control groups were sparsely dispersed in             |
| 539 | the tumour metastasis niche (Fig. 5F). Under the effect of FOL-M@NLP, the                                   |
| 540 | infiltration of PD-1 <sup>+</sup> cells and PD-L1 <sup>+</sup> cells within the tumour metastasis niche was |
| 541 | greater than that in the NS group (Fig. S18).   |
| 542 | To summarize, FOL-M@NLP showed adequate tumour suppression relative to the                                  |
| 543 | other controls. In TDLNs and the spleen, the two major sites where immune responses                         |
| 544 | occur, APCs, after phagocytosis of this vaccine and effective activation, can present                       |
| 545 | processed epitopes to T cells, which can be fully activated, proliferate, differentiate into                |
| 546 | effector T cells, migrate to the tumour metastasis niche and fully infiltrate under the                     |
| 547 | action of chemokines to enhance attack on target cells and inhibit the negative                             |
| 548 | regulation of immunity. Moreover, innate immune cells are also activated and fully                          |
| 549 | infiltrate in the tumour metastasis niche, further enhancing tumour suppression.                            |

| 551 | 3.6. Analysis of molecular biological changes in the tumour metastasis niche induced      |
|-----|---|
| 552 | by FOL-M@NLP  |
| 553 | To clarify the changes in the tumour metastasis niche after the application of FOL-       |
| 554 | M@NLP at the molecular biology level, RNA sequencing was performed on lungs with          |
| 555 | melanoma metastases. Compared with NS, the application of FOL-M@NLP                       |
| 556 | significantly upregulated 1086 genes and downregulated 79 genes. Some key genes           |
| 557 | involved in antitumour immune functions were upregulated after the application of         |
| 558 | FOL-M@NLP (Fig. 7A). Heatmap analysis revealed that most of the genes associated          |
| 559 | with positive immunity in the tumour metastasis niche of the FOL-M@NLP group were         |
| 560 | highly expressed compared with those in the NS group (Fig. 7B). KEGG pathway              |
| 561 | enrichment analysis revealed immune pathways related to antigen presentation, the         |
| 562 | binding of cytokines to their receptors, the differentiation of helper T cells, and the   |
| 563 | cytotoxicity of NK cells, as well as signalling pathways involving cytokines and          |
| 564 | chemokines in the immune process (Fig. 7C). GO analysis was performed to enrich           |
| 565 | terms related to biological processes (BP), cellular components (CC) and molecular        |
| 566 | functions (MF). BP enrichment involved adaptive immune processes, such as                 |
| 567 | phagocytosis, antigen processing and presentation, T-cell activation and differentiation, |
| 568 | and cell killing, as well as immune processes through the tumour necrosis factor          |
| 569 | superfamily and NK cells. CC analysis enriched Inflammatory complexes, especially         |
| 570 | AIM2 inflammasome complex, in immune cells, MHC complexes on the surface of               |
| 571 | APCs, T cell receptors (TCRs), and immune synapses. According to the MF analysis,         |

molecules that perform positive immune functions during adaptive and innate immunity were also enriched (**Fig. 7D**). The hub genes screened by PPI network analysis were *Ifng, Cd4, Itgax, Sell, Gzmb, Ptprc* and *Ccr7* (**Fig. 7E**). *Ifng*, encoding interferon-γ that induces specific immune response; *Cd4*, encoding surface marker of helper T-cells that regulate cytotoxic immune response; *Itgax*, encoding CD11c and having integrinbinding activity and receptor tyrosine kinase-binding activity; *Sell*, encoding L-selectin (CD62L), which acts as lymph node homing receptor; *Gzmb*, encoding granzyme B that induces apoptosis of target cells; *Ptprc*, participating in the positive regulation of T cell activation and the regulation of protein phosphorylation; *Ccr7*, Enhancement of C-C chemokine receptor activity involved in positive regulation of immune response (Corroborated in NCBI database). All the hub genes play positive roles in different stages of antitumour immunity. At the molecular biology level, the biovaccine FOL-M@NLP reinforced each stage of the adaptive immune response while also facilitating the destructive function exerted by the innate immunity against tumour cells.

#### 3.7. Recurrence prevention of FOL-M@NLP in postoperative tumour model

The postoperative model was designed to observe the ability of FOL-M@NLP to prevent recurrence after tumour resection. Model construction, treatment planning, and observations are shown in **Fig. 8A**. The body weights of the mice in all 6 groups slowly increased after surgery, indicating that the mice were in a state of slow recovery after surgical stress. No statistically significant differences were found among the body weights of the 6 groups of mice at each time point, indicating that the safety of the 6

| groups of drugs was good and that none of them affected the postoperative recovery of     |
|---|
| the mice (Fig. 8B). Tumour growth curves indicated that FOL-M@NLP inhibited               |
| tumour growth better than other groups (Fig. 8C). Within the first 30 days after surgery, |
| the mice in the NS, NLP, FOLactis, and FOL-M groups were all tumour-bearing, and          |
| all the tumours showed significant growth, whereas 1 mouse in the FOL-M+NLP group         |
| and 3 in the FOL-M@NLP group were in a non-recurrence state (Fig. 8D). All the mice       |
| in the NS, NLP, FOLactis, and FOL-M groups reached the survival endpoints on              |
| postoperative days 42, 42, 40, and 48, respectively, and there was no statistically       |
| significant difference in survival among the groups. At postoperative day 90, 1 mouse     |
| (20%) was still alive in the FOL-M+NLP group, and 2 mice (40%) were alive in the          |
| FOL-M@NLP group (Fig. 8E). None of these 3 mice experienced tumour recurrence.            |
| Both FOL-M+NLP and FOL-M@NLP prevented postoperative tumour recurrence and                |
| improved survival in mice, whereas FOL-M@NLP was more effective than the other 4          |
| treatments were.  |
| On postoperative day 90, rechallenge experiments were performed. The tumour growth        |
| was slower in the FOL-M+NLP and FOL-M@NLP groups than in the control group in             |
| the first 30 days after rechallenge (Fig. 8F). 1 mouse in the FOL-M@NLP group was         |
| not tumour-bearing until day 29 after rechallenge (Figs. 8G and S19). All the mice in     |
| the control, FOL-M+NLP and FOL-M@NLP groups reached the survival endpoints on             |
| days 37, 38 and 55 after rechallenge, respectively (Fig. 8H). After FOL-M@NLP             |
| effectively prevented tumour recurrence, it also left immune memory in the body, which    |
| could exert an inhibitory effect on tumour growth when encountering the same tumour       |

| 616 | rechal | lenge. |
|-----|--------|--------|
|     |        |        |

3.8. Preventive effect exerted by FOL-M@NLP against tumour

In addition to good tumour inhibition and prevention of postoperative recurrence, the vaccine also exhibited good prevention against tumours. After 4 times of vaccination and being challenged with tumour (Fig. 9A), there was no significant difference in the weight changes of the mice in each group during the observation process (Fig. 9B), and the tumour growth of the mice that were vaccinated with NLP was not significantly different from that of the NS group, whereas after the application of FOL-M@NLP, the growth of the tumours was significantly inhibited compared with that of the NS group and the NLP group, which showed the preventive potency of the vaccine against tumours (Fig. 9C, 9D and S20).

3.9. Specific immune response and biosafety of FOL-M@NLP

A mouse vaccination model was constructed to verify immune response specificity and biosafety (Fig. 9E). The spleen lymphocytes of mice were harvested as effector cells. 4T1-NY-ESO-1 cells were selected as target cells. Splenocytes that received NLP stimulation induced more IFN-γ spots after restimulation with NY-ESO-1 antigen expressed by target cells, whereas splenocytes that had received FOL-M@NLP stimulation showed a significant increase in NY-ESO-1-specific IFN-γ secretion with exposure to the antigen (Fig. 9F). Compared with other groups, the effector cells had a significant destructive effect on target cells after they were stimulated with FOL-

M@NLP (15.93±0.91%). After stimulation with FOL-M+NLP, effector cells were also able to effectively destroy target cells (11.41±0.51%), but the destruction effect was inferior to that of FOL-M@NLP (Fig. 9G and S21A). For comparison, wild-type 4T1 cells were also selected as target cells and cocultured with effector cells. The difference in the proportion of destroyed target cells among the 6 groups was not statistically significant (Fig. 9H and S21B). On the basis of these results, the main target of FOL-M@NLP was the NY-ESO-1 antigen expressed by target cells. Biochemical analysis revealed no significant differences in alanine aminotransferase, aspartate aminotransferase, alkaline phosphatase, urea, or creatinine among the 6 groups (Fig. S22). In addition, no evidence demonstrated that the main organs of the mice (heart, liver, spleen, lung and kidney) in these 6 groups were damaged (Fig. S23). The above results revealed the favourable biosafety of the biovaccine.

#### 4. Discussion

In this study, we synthesized a biovaccine targeting the cancer testis antigen NY-ESO-1. The reason why the NY-ESO-1 protein was not selected but the NLP was that the NY-ESO-1 protein is easily folded during the synthesis process, resulting in the antigenic epitope being difficult to fully expose; thus, the recombinant protein is difficult to be recognized by the APCs, whereas the peptide with only several dozens of amino acids can directly expose the antigenic epitopes to the APCs, making it easier to bind to TCR and activate the downstream immune response [2, 22, 23]. In our study, 3 NY-ESO-1 multiepitope long peptides screened by bioinformatic methods exhibited

affinities to MHC I and II.

660

Naked peptides usually have a short half-life and poor stability in vivo. To overcome 661 these limitations, adjuvants need to be used in combination [1]. Baumgaertner et al. 662 combined NY-ESO-1 long peptide (79-108) with Montanide and the TLR3 agonist 663 CpG-ODN in patients with stage III/IV melanoma and reported that it could induce 664 integrated, robust and functional CD8<sup>+</sup> and CD4<sup>+</sup> T-cell responses in patients [5]. 665 FOLactis, an engineered *Lactococcus lactis* strain that secretes Flt3L and OX40L fusion 666 proteins designed by our team previously, was injected in situ to regulate key 667 668 components of the antitumour immune response [8]. Metal elements, such as magnesium, can effectively activate the immune response [24]. On the basis of the 669 above results, we developed a MOF composed of magnesium and 2-methylimidazole. 670 The MOF was loaded on the surface of FOLactis and loading the NY-ESO-1 671 multiepitope long peptides into the framework, and the biovaccine FOL-M@NLP was 672 synthesized. 673 674 We characterized the synthesized vaccine with a series of properties. The particle-like roughness of the FOL-M@NLP surface and Mg2+ distributed on the bacterium has 675 proved that MOF was successfully loaded on FOLactis. The 3 peptides exhibited 676 distinct properties of EE and could be gradually released from the biovaccine in the 677 simulated immune microenvironment. The loading of MOF onto FOLactis did not 678 significantly affect the activity of FOLactis itself. The activity of cells was also not 679 680 affected after coincubation with the biovaccine, and the biovaccine showed low toxicity on cells. 681

| 682 | After entering the body, antigen peptides are taken up and processed by APCs. The      |
|-----|--|
| 683 | pMHC on the surface of mature APCs can bind to the surface receptors of naive T cells. |
| 684 | The immunoreceptor tyrosine activation motif (ITAM) on the surface of T lymphocytes    |
| 685 | is phosphorylated, initiating the molecular signals of T lymphocyte activation [25].   |
| 686 | Moreover, the signalling of costimulatory molecules on the surface of DC cells and T   |
| 687 | lymphocytes can further promote the activation of T lymphocytes, such as intercellular |
| 688 | adhesion molecule 1 (ICAM-1)/leukocyte function antigen-1 (LFA-1) and                  |
| 689 | CD80/CD86/CD28 [26, 27]. We simulated the recognition and uptake of the vaccine        |
| 690 | by APCs, the maturation of APCs, and the activation of T cells in vitro. NLP can be    |
| 691 | efficiently taken up by BMDCs, while recognition and uptake of FOL-M@NLP by            |
| 692 | BMDCs are quicker. PAMPs on FOL-M@NLP can be recognized and bound by pattern           |
| 693 | recognition receptors on DCs, mainly TLR1, TLR2 and TLR6 [8], and then accelerate      |
| 694 | the uptake process. Under the combined effect of multiepitope long peptides and        |
| 695 | PAMPs on FOLactis, DCs can rapidly differentiate into a mature state after             |
| 696 | phagocytosis of FOL-M@NLP. T cells were also rapidly activated under stimulation       |
| 697 | with pMHC presented by mature DCs, and the costimulatory signal. Compared with         |
| 698 | NLP alone or FOLactis alone, FOL-M@NLP increased the efficiency of the immune          |
| 699 | response in vitro.   |
| 700 | Melanoma is a malignant neoplasm that is likely to metastasize and sometimes           |
| 701 | expresses the NY-ESO-1 antigen [3, 4]. Thus, NY-ESO-1-positive primary melanoma        |
| 702 | model and lung metastasis model were established to validate the inhibition of tumour  |
| 703 | progression and metastasis by FOL-M@NLP. FOL-M@NLP significantly inhibited the         |

705

706

707

708

709

710

711

712

713

714

715

716

717

718

719

720

721

722

723

724

725

process of neoplasm progression, as evidenced by the observation of primary tumours and metastases. FOL-M@NLP can adequately exert an immune response at sites of immune cell differentiation, primarily the TDLN and spleen, by activating settled T cells after antigen presentation and allowing them to differentiate into effector-ready subpopulations. DCs settled in tumour sites may ingest tumour antigens or exogenous antigens, mature and upregulate MHC I and MHC II expression to enhance classical antigen presentation and cross-presentation. Guided by chemokines, T cells reach TME or the tumour metastasis niche, were activated again and rapidly exert specific cytotoxicity upon encountering antigens expressed in the tumour, activate the caspase cascade reaction and induce apoptosis in target cells through the perforin-granzyme pathway as well as the Fas-FasL pathway [28]. Tregs are suppressor immune cells that express TGF-β, which suppresses the antigen presentation of DCs as well as the activation of NK cells and macrophages [29, 30]. TGF-β also induces immune escape in tumours via stromal synthesis and vascular production [31]. CD8<sup>+</sup> T cells and Th1 cells can suppress the populations and functions of Treg cells by secreting IFN-y [32]. In this study, FOL-M@NLP successfully promoted the infiltration of IFN-γ<sup>+</sup> CD8<sup>+</sup> T cells in TME and effector memory CD8<sup>+</sup> T cells in the metastasis niche, which could inhibit the differentiation of helper T cells to Tregs. After destruction by cytotoxic T cells, tumour cells release damage-associated molecular patterns (DAMPs). DAMPs can act as endogenous adjuvants to reactivate APCs, cross-present tumour antigens and act as amplifiers of the T-cell immune response [33]. DAMPs also fully mobilize the capacity of innate immunity [34-36], which was verified in our study by the infiltration

| of NK cells and macrophage polarization in the tumour metastasis niche after the                                |
|---|
| application of FOL-M@NLP. After vaccination with FOL-M@NLP, IFN- $\gamma^+$ cells could                         |
| aggregate, with specific cytotoxicity enhanced, maturation of DCs promoted, the                                 |
| expression of MHC I and MHC II molecules upregulated, macrophage polarization                                   |
| toward the classically activated type promoted and the level of vascular endothelial                            |
| growth factor regulated to limit angiogenesis, etc [32]. After the application of FOL-                          |
| M@NLP, the infiltration of PD-1 <sup>+</sup> cells and PD-L1 <sup>+</sup> cells into the tumour site increased, |
| and the immune microenvironment transformed from a "cold" state to a "hot" state [37].                          |
| Cytokines in TME exert multiple functions in immunity. The presence of IL-4 and IL-                             |
| 13 in TME promotes "M2-like" tumour-associated macrophages proliferation, induce                                |
| CD4 <sup>+</sup> T cells to skew towards Th2 polarization and inhibit the cytotoxic function of                 |
| CD8 <sup>+</sup> T cells [38, 39]. IL-10 blunts APC response to antigen stimulation, inhibit the                |
| proliferation and function of CD4 <sup>+</sup> T cells to induce nonresponsiveness and anergy [40,              |
| 41]. IL-6 acts on tumour cells to induce the expression of STAT3, which further induce                          |
| the expression of factors that promote angiogenesis, invasiveness or metastasis, and                            |
| immunosuppression. STAT3 induced by IL-6 often exerts negative regulatory effects                               |
| on DCs, effector T cells and NK cells, while positively regulate Tregs and myeloid-                             |
| derived suppressor cells, resulting in downmodulation of antitumour immunity [42,                               |
| 43]. With the administration of FOL-M@NLP, IL-4, IL-13, IL-10 and IL-6 in TME have                              |
| downregulated and the immune microenvironment has improved.   |
| Through molecular biology studies, we found that many immune-related genes, which                               |
| are overeynressed in the tumour metastasis niche, were unregulated following the                                |

| application of FOL-M@NLP. KEGG pathway enrichment involved major pathways of                  |
|---|
| cellular and molecular signalling and the enhancement of innate and adaptive immunity,        |
| which was corroborated by GO enrichment term analysis of BP, CC and MF. The above             |
| results confirm on multiple levels that the biovaccine FOL-M@NLP can adequately               |
| inhibit tumour metastasis by activating innate and adaptive immunity.                         |
| We also developed a postoperative model and a prevention model to assess the role of          |
| the vaccine in preventing tumour and recurrence. FOL-M@NLP effectively inhibited              |
| tumour growth without affecting recovery after encountering surgical stress and was           |
| effective in preventing tumour recurrence and prolonging survival. The results of the         |
| rechallenge experiments illustrated that the application of FOL-M@NLP could leave             |
| immune memory in vivo and could exert immune efficacy after encountering the same             |
| antigen. FOL-M@NLP also has a good potency to prevent tumours. This biovaccine                |
| was confirmed to be specific when encounters cells expressing NY-ESO-1 and had a              |
| favourable safety profile.  |
| There are several limitations in our study. First, without the help of adjuvants, the         |
| individual effects of the 3 peptides we screened were not prominent. Thus, the                |
| conjugation of adjuvants was indispensable. Second, some immunosuppressive genes,             |
| such as Cd274, which encodes PD-L1, are also highly expressed. After the application          |
| of the vaccine, the degree of effector T-cell infiltration in the metastasis niche increased, |
| and the immune state of tumour transformed from "cold" to "hot", resulting in a high          |
| tumour mutational burden and increased PD-L1 expression [37]. The application of              |
| anti-PD-L1 monoclonal antibodies may block this immunosuppressive signalling                  |

pathway and positively modulate immune efficacy. Third, although vaccines can suppress tumours through immune effects, their destructive effects are still not as strong as those of chemotherapy and radiotherapy on tumours. Some chemotherapeutic drugs and radiotherapy can induce immunogenic tumour cell death, release more DAMPs, and amplify the antitumour immune effect; thus, the effect of the combined application of this biovaccine and chemotherapy/radiotherapy is also a direction that needs in-depth research.

### 5. Conclusion

In this study, a combination of engineered bacteria with multiepitope antigenic peptides was developed to construct an efficient tumour vaccine. We screened three multiepitope long peptides from the cancer testis antigen NY-ESO-1 and used the engineered bacteria FOLactis as a carrier and adjuvant to construct a multiepitope long peptide biovaccine. The experimental results revealed that the biovaccine could quickly enhance the endocytosis efficiency of APCs, activate the immune response of immature DCs and naive T cells, enhance the expansion of immune cells in immune organs and the infiltration of immune cells in TME or tumour metastasis niche, inhibit tumour growth and recurrence, and prolong the survival of tumour-bearing mice. The biovaccine construction strategy provides new ideas for the preparation of tumour vaccines.

## **CRediT** authorship contribution statement

Chunyi Li: Writing-original draft, Visualization, Validation, Resources, Project

| 792 | administration, Methodology, Investigation, Formal analysis, Data curation, and       |
|-----|---|
| 793 | Conceptualization. Kongcheng Wang: Project administration, Investigation,             |
| 794 | Conceptualization. Jie Shao: Project administration, Methodology, Conceptualization.  |
| 795 | Junmeng Zhu: Project administration, Methodology, Resources. Yaohua·Ke: Project       |
| 796 | administration, Methodology, Conceptualization. Baorui Liu: Writing-review &          |
| 797 | editing, Resources, Software, Supervision, Project administration, Methodology,       |
| 798 | Investigation, Funding acquisition, Formal analysis, Conceptualization. Lanqi Cen:    |
| 799 | Writing-review & editing, Resources, Software, Supervision, Project administration,   |
| 800 | Investigation, Formal analysis, Conceptualization.                                    |
| 801 |   |
| 802 | Ethics approval   |
| 803 | All animal experiments were approved by the Laboratory Animal Care and Use            |
| 804 | Committee of the Affiliated Nanjing Drum Tower Hospital of Nanjing University         |
| 805 | Medical School (2023AE01063) and were carried out in compliance with all relevant     |
| 806 | ethical regulations.  |
| 807 |   |
| 808 | Declaration of competing interest   |
| 809 | The authors declare that they have no known competing financial interests or personal |
| 810 | relationships that could have appeared to influence the work reported in this paper.  |
| 811 |   |
| 812 | Consent for publication   |
| 813 | All the authors agree to the publication of this work.                                |

| 814 |   |
|-----|---|
| 815 | Funding information   |
| 816 | This work was financially supported by the National Natural Science Foundation of       |
| 817 | China (No. 82272811 and No. 824B2092), Jiangsu Provincial Medical Key Discipline        |
| 818 | (ZDXK202233), Nanjing Medical Key Laboratory of Oncology, Jiangsu Province Key          |
| 819 | Research and Development Program (BE2023654) and Nanjing Jiangbei New Area              |
| 820 | Key Research and Development Program.   |
| 821 |   |
| 822 | Data availability   |
| 823 | Data will be made available on request.   |
| 824 |   |
| 825 | Reference   |
| 826 | [1] L. Buonaguro, M. Tagliamonte, Peptide-based vaccine for cancer therapies, Front     |
| 827 | Immunol 14 (2023) 1210044, https://doi.org/10.3389/fimmu.2023.1210044.                  |
| 828 | [2] H. Zhou, Y. Ma, F. Liu, B. Li, D. Qiao, P. Ren, M. Wang, Current advances in cancer |
| 829 | vaccines targeting NY-ESO-1 for solid cancer treatment, Front Immunol 14 (2023)         |
| 830 | 1255799, https://doi.org/10.3389/fimmu.2023.1255799.                                    |
| 831 | [3] A. Raza, M. Merhi, V.P. Inchakalody, R. Krishnankutty, A. Relecom, S. Uddin, S.     |
| 832 | Dermime, Unleashing the immune response to NY-ESO-1 cancer testis antigen as a          |
| 833 | potential target for cancer immunotherapy, J Transl Med 18 (1) (2020) 140,              |
| 834 | https://doi.org/10.1186/s12967-020-02306-y.   |
| 835 | [4] R. Thomas, G. Al-Khadairi, J. Roelands, W. Hendrickx, S. Dermime, D. Bedognetti,    |

- J. Decock, NY-ESO-1 Based Immunotherapy of Cancer: Current Perspectives, Front
- 837 Immunol 9 (2018) 947, https://doi.org/10.3389/fimmu.2018.00947.
- 838 [5] P. Baumgaertner, C. Costa Nunes, A. Cachot, H. Maby-El Hajjami, L. Cagnon, M.
- Braun, L. Derré, J.P. Rivals, D. Rimoldi, S. Gnjatic, S. Abed Maillard, P. Marcos
- Mondéjar, M.P. Protti, E. Romano, O. Michielin, P. Romero, D.E. Speiser, C. Jandus,
- Vaccination of stage III/IV melanoma patients with long NY-ESO-1 peptide and CpG-
- B elicits robust CD8(+) and CD4(+) T-cell responses with multiple specificities
- including a novel DR7-restricted epitope, Oncoimmunology 5 (10) (2016) e1216290,
- 844 https://doi.org/10.1080/2162402x.2016.1216290.
- 845 [6] S. Apostólico Jde, V.A. Lunardelli, F.C. Coirada, S.B. Boscardin, D.S. Rosa,
- 846 Adjuvants: Classification, Modus Operandi, and Licensing, J Immunol Res 2016
- 847 (2016) 1459394, https://doi.org/10.1155/2016/1459394.
- [7] C. Hou, B. Yi, J. Jiang, Y.F. Chang, X. Yao, Up-to-date vaccine delivery systems:
- robust immunity elicited by multifarious nanomaterials upon administration through
- diverse routes, Biomater Sci 7 (3) (2019) 822-835, https://doi.org/10.1039/c8bm01197d.
- [8] J. Zhu, Y. Ke, Q. Liu, J. Yang, F. Liu, R. Xu, H. Zhou, A. Chen, J. Xiao, F. Meng, L.
- Yu, R. Li, J. Wei, B. Liu, Engineered Lactococcus lactis secreting Flt3L and OX40
- ligand for in situ vaccination-based cancer immunotherapy, Nat Commun 13 (1) (2022)
- 7466, https://doi.org/10.1038/s41467-022-35130-7.
- 855 [9] T. Kawai, M. Ikegawa, D. Ori, S. Akira, Decoding Toll-like receptors: Recent
- insights and perspectives in innate immunity, Immunity 57 (4) (2024) 649-673,
- 857 https://doi.org/10.1016/j.immuni.2024.03.004.

- 858 [10] L.M. Howell, N.S. Forbes, Bacteria-based immune therapies for cancer treatment,
- 859 Semin Cancer Biol 86 (Pt 2) (2022) 1163-1178,
- 860 https://doi.org/10.1016/j.semcancer.2021.09.006.
- 861 [11] K. Garbacz, Anticancer activity of lactic acid bacteria, Semin Cancer Biol 86 (Pt
- 3) (2022) 356-366, https://doi.org/10.1016/j.semcancer.2021.12.013.
- 863 [12] C. Moussion, L. Delamarre, Antigen cross-presentation by dendritic cells: A
- critical axis in cancer immunotherapy, Semin Immunol 71 (2024) 101848,
- 865 https://doi.org/10.1016/j.smim.2023.101848.
- 866 [13] G.J. Webb, G.M. Hirschfield, P.J. Lane, OX40, OX40L and Autoimmunity: a
- 867 Comprehensive Review, Clin Rev Allergy Immunol 50 (3) (2016) 312-32,
- 868 https://doi.org/10.1007/s12016-015-8498-3.
- 869 [14] Y. He, J. Li, W. Mao, D. Zhang, M. Liu, X. Shan, B. Zhang, C. Zhu, J. Shen, Z.
- Deng, Z. Wang, W. Yu, Q. Chen, W. Guo, P. Su, R. Lv, G. Li, G. Li, B. Pei, L. Jiao, G.
- Shen, Y. Liu, Z. Feng, Y. Su, Y. Xie, W. Di, X. Liu, X. Yang, J. Wang, J. Qi, Q. Liu, Y.
- Han, J. He, J. Cai, Z. Zhang, F. Zhu, D. Du, HLA common and well-documented alleles
- in China, Hla 92 (4) (2018) 199-205, https://doi.org/10.1111/tan.13358.
- 874 [15] B. Reynisson, B. Alvarez, S. Paul, B. Peters, M. Nielsen, NetMHCpan-4.1 and
- NetMHCIIpan-4.0: improved predictions of MHC antigen presentation by concurrent
- motif deconvolution and integration of MS MHC eluted ligand data, Nucleic Acids Res
- 48 (W1) (2020) W449-w454, https://doi.org/10.1093/nar/gkaa379.
- 878 [16] S. Kaabinejadian, C. Barra, B. Alvarez, H. Yari, W.H. Hildebrand, M. Nielsen,
- 879 Accurate MHC Motif Deconvolution of Immunopeptidomics Data Reveals a

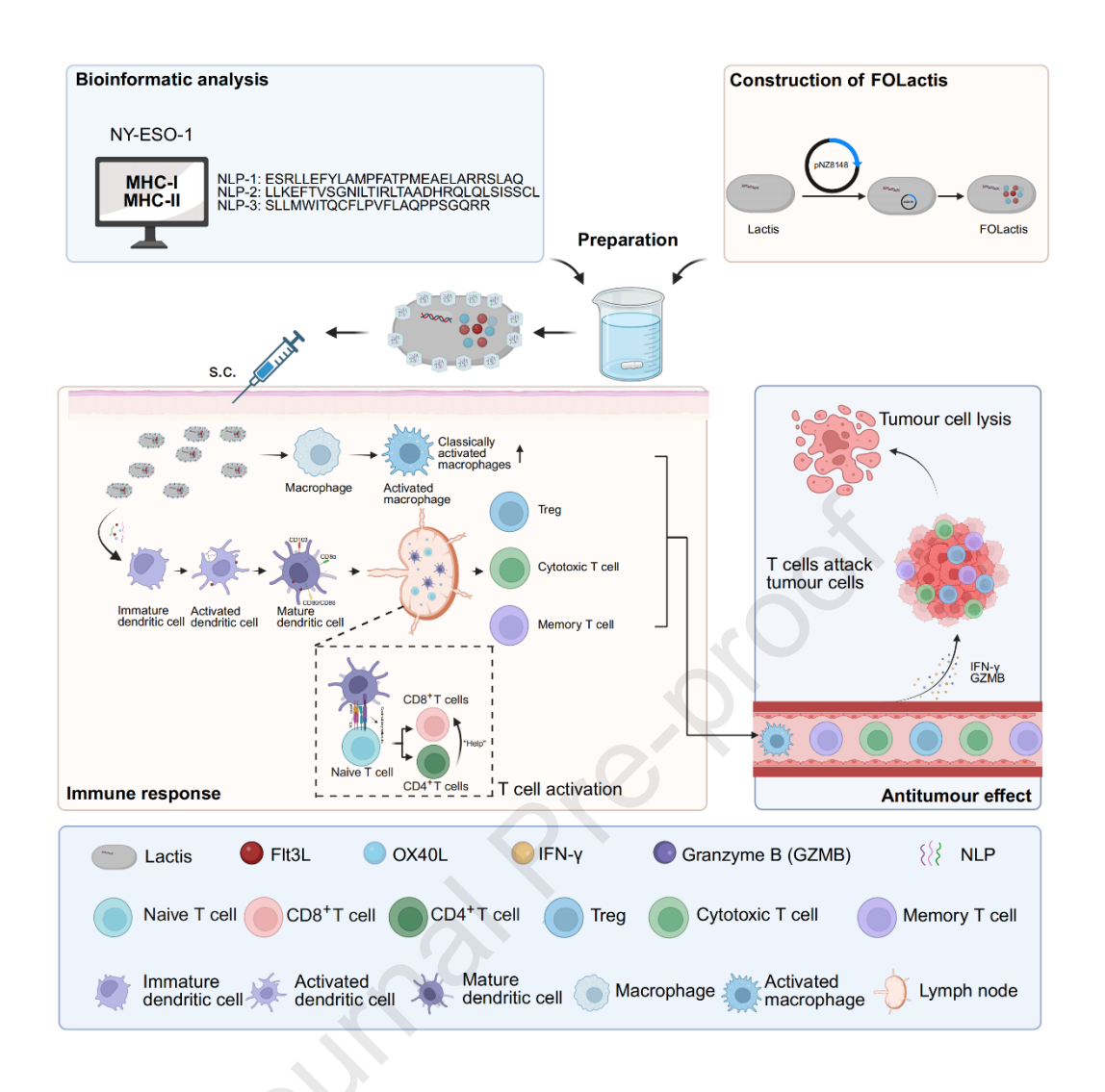
- 880 Significant Contribution of DRB3, 4 and 5 to the Total DR Immunopeptidome, Front
- 881 Immunol 13 (2022) 835454, https://doi.org/10.3389/fimmu.2022.835454.
- 882 [17] H. Hu, Y. Lin, B. Yang, X. Wen, P. Ma, X.J. Loh, Z. Luo, Z. Li, Y.-L. Wu,
- 883 Biomineralization-inspired functional biomaterials: From principles to practice,
- 884 Chemical Engineering Journal 504 (2025) 158624,
- 885 https://doi.org/https://doi.org/10.1016/j.cej.2024.158624.
- 886 [18] Q. Wang, L. Hu, X. Wang, R. Tang, Expanding from materials to biology inspired
- by biomineralization, Interdisciplinary Materials 3 (2) (2024) 165-188,
- 888 https://doi.org/https://doi.org/10.1002/idm2.12144.
- [19] J. Guo, F. Gao, F. Zhang, X. Zhao, R. Zhao, Biomineralization-Driven Advances
- in Materials Science and Biomedical Engineering, JACS Au 5 (9) (2025) 4134-4154,
- 891 https://doi.org/10.1021/jacsau.5c00669.
- [20] C. Wang, L. Zhong, J. Xu, Q. Zhuang, F. Gong, X. Chen, H. Tao, C. Hu, F. Huang,
- N. Yang, J. Li, Q. Zhao, X. Sun, Y. Huo, Q. Chen, Y. Zhao, R. Peng, Z. Liu, Oncolytic
- 894 mineralized bacteria as potent locally administered immunotherapeutics, Nat Biomed
- 895 Eng 8 (5) (2024) 561-578, https://doi.org/10.1038/s41551-024-01191-w.
- 896 [21] S. Yan, X. Zeng, Y. Wang, B.F. Liu, Biomineralization of Bacteria by a Metal-
- 897 Organic Framework for Therapeutic Delivery, Adv Healthc Mater 9 (12) (2020)
- 898 e2000046, https://doi.org/10.1002/adhm.202000046.
- 899 [22] O. Klein, I.D. Davis, G.A. McArthur, L. Chen, A. Haydon, P. Parente, N.
- 900 Dimopoulos, H. Jackson, K. Xiao, E. Maraskovsky, W. Hopkins, R. Stan, W. Chen, J.
- 901 Cebon, Low-dose cyclophosphamide enhances antigen-specific CD4(+) T cell

- 902 responses to NY-ESO-1/ISCOMATRIX<sup>TM</sup> vaccine in patients with advanced melanoma,
- 903 Cancer Immunol Immunother 64 (4) (2015) 507-18, https://doi.org/10.1007/s00262-
- 904 015-1656-x.
- 905 [23] A. Pavlick, A.B. Blazquez, M. Meseck, M. Lattanzi, P.A. Ott, T.U. Marron, R.M.
- 906 Holman, J. Mandeli, A.M. Salazar, C.B. McClain, G. Gimenez, S. Balan, S. Gnjatic,
- 907 R.L. Sabado, N. Bhardwaj, Combined Vaccination with NY-ESO-1 Protein, Poly-ICLC,
- and Montanide Improves Humoral and Cellular Immune Responses in Patients with
- 909 High-Risk Melanoma, Cancer Immunol Res 8 (1) (2020) 70-80,
- 910 https://doi.org/10.1158/2326-6066.Cir-19-0545.
- 911 [24] X. Chen, L. Cen, Q. Liu, Y. Chu, X. Feng, Y. Ke, Z. Zhang, H. Dai, S. Huang, B.
- 912 Liu, X. Qian, A dual-adjuvant neoantigen nanovaccine loaded with imiquimod and
- 913 magnesium enhances anti-tumor immune responses of melanoma, Biomater Sci 10 (23)
- 914 (2022) 6740-6748, https://doi.org/10.1039/d2bm01340a.
- 915 [25] W.W. Schamel, B. Alarcon, S. Minguet, The TCR is an allosterically regulated
- 916 macromolecular machinery changing its conformation while working, Immunol Rev
- 917 291 (1) (2019) 8-25, https://doi.org/10.1111/imr.12788.
- 918 [26] A. Gérard, A.P. Cope, C. Kemper, R. Alon, R. Köchl, LFA-1 in T cell priming,
- 919 differentiation, and effector functions, Trends Immunol 42 (8) (2021) 706-722,
- 920 https://doi.org/10.1016/j.it.2021.06.004.
- 921 [27] N. Dadwal, C. Mix, A. Reinhold, A. Witte, C. Freund, B. Schraven, S. Kliche, The
- 922 Multiple Roles of the Cytosolic Adapter Proteins ADAP, SKAP1 and SKAP2 for
- 923 TCR/CD3 -Mediated Signaling Events, Front Immunol 12 (2021) 703534,

- 924 https://doi.org/10.3389/fimmu.2021.703534.
- 925 [28] H. Raskov, A. Orhan, J.P. Christensen, I. Gögenur, Cytotoxic CD8(+) T cells in
- 926 cancer and cancer immunotherapy, Br J Cancer 124 (2) (2021) 359-367,
- 927 https://doi.org/10.1038/s41416-020-01048-4.
- 928 [29] J. Wang, X. Zhao, Y.Y. Wan, Intricacies of TGF-β signaling in Treg and Th17 cell
- 929 biology, Cell Mol Immunol 20 (9) (2023) 1002-1022, https://doi.org/10.1038/s41423-
- 930 023-01036-7.
- 931 [30] E. Batlle, J. Massagué, Transforming Growth Factor-β Signaling in Immunity and
- 932 Cancer, Immunity 50 (4) (2019) 924-940,
- 933 https://doi.org/10.1016/j.immuni.2019.03.024.
- 934 [31] L.F. Loffredo, T.M. Savage, O.R. Ringham, N. Arpaia, Treg-tissue cell interactions
- 935 in repair and regeneration, J Exp Med 221 (6) (2024)
- 936 https://doi.org/10.1084/jem.20231244.
- 937 [32] A.M. Gocher, C.J. Workman, D.A.A. Vignali, Interferon-y: teammate or opponent
- 938 in the tumour microenvironment?, Nat Rev Immunol 22 (3) (2022) 158-172,
- 939 https://doi.org/10.1038/s41577-021-00566-3.
- 940 [33] G.Y. Jang, J.W. Lee, Y.S. Kim, S.E. Lee, H.D. Han, K.J. Hong, T.H. Kang, Y.M.
- 941 Park, Interactions between tumor-derived proteins and Toll-like receptors, Exp Mol
- 942 Med 52 (12) (2020) 1926-1935, https://doi.org/10.1038/s12276-020-00540-4.
- 943 [34] E. Guilbaud, G. Kroemer, L. Galluzzi, Calreticulin exposure orchestrates innate
- 944 immunosurveillance, Cancer Cell 41 (6) (2023) 1014-1016,
- 945 https://doi.org/10.1016/j.ccell.2023.04.015.

- 946 [35] M. Ma, W. Jiang, R. Zhou, DAMPs and DAMP-sensing receptors in inflammation
- 947 and diseases, Immunity 57 (4) (2024) 752-771,
- 948 https://doi.org/10.1016/j.immuni.2024.03.002.
- 949 [36] J. Xue, J.S. Suarez, M. Minaai, S. Li, G. Gaudino, H.I. Pass, M. Carbone, H. Yang,
- 950 HMGB1 as a therapeutic target in disease, J Cell Physiol 236 (5) (2021) 3406-3419,
- 951 https://doi.org/10.1002/jcp.30125.
- 952 [37] G.R. Khosravi, S. Mostafavi, S. Bastan, N. Ebrahimi, R.S. Gharibvand, N.
- 953 Eskandari, Immunologic tumor microenvironment modulators for turning cold tumors
- 954 hot, Cancer Commun (Lond) 44 (5) (2024) 521-553,
- 955 https://doi.org/10.1002/cac2.12539.
- 956 [38] Z.J. Bernstein, A. Shenoy, A. Chen, N.M. Heller, J.B. Spangler, Engineering the
- 957 IL-4/IL-13 axis for targeted immune modulation, Immunol Rev 320 (1) (2023) 29-57,
- 958 https://doi.org/10.1111/imr.13230.
- 959 [39] M. Jaén, Á. Martín-Regalado, R.A. Bartolomé, J. Robles, J.I. Casal, Interleukin 13
- 960 receptor alpha 2 (IL13Rα2): Expression, signaling pathways and therapeutic
- applications in cancer, Biochim Biophys Acta Rev Cancer 1877 (5) (2022) 188802,
- 962 https://doi.org/10.1016/j.bbcan.2022.188802.
- 963 [40] M.A. Salkeni, A. Naing, Interleukin-10 in cancer immunotherapy: from bench to
- 964 bedside, Trends Cancer 9 (9) (2023) 716-725,
- 965 https://doi.org/10.1016/j.trecan.2023.05.003.
- 966 [41] M. Saraiva, P. Vieira, A. O'Garra, Biology and therapeutic potential of interleukin-
- 967 10, J Exp Med 217 (1) (2020) https://doi.org/10.1084/jem.20190418.

| 968 | [42] D.E. Johnson, R.A. O'Keefe, J.R. Grandis, Targeting the IL-6/JAK/STAT3               |
|-----|---|
| 969 | signalling axis in cancer, Nat Rev Clin Oncol 15 (4) (2018) 234-248,                      |
| 970 | https://doi.org/10.1038/nrclinonc.2018.8.   |
| 971 | [43] S.A. Jones, B.J. Jenkins, Recent insights into targeting the IL-6 cytokine family in |
| 972 | inflammatory diseases and cancer, Nat Rev Immunol 18 (12) (2018) 773-789,                 |
| 973 | https://doi.org/10.1038/s41577-018-0066-7.  |
| 974 |   |
| 975 |   |
| 976 |   |
| 977 |   |
|     |   |
|     |   |
|     |   |
|     |   |
|     |   |



**Scheme 1.** Schematic diagram of the tumour vaccine FOL-M@NLP synthesized, and analysis of its immune efficacy. Created in BioRender.com.

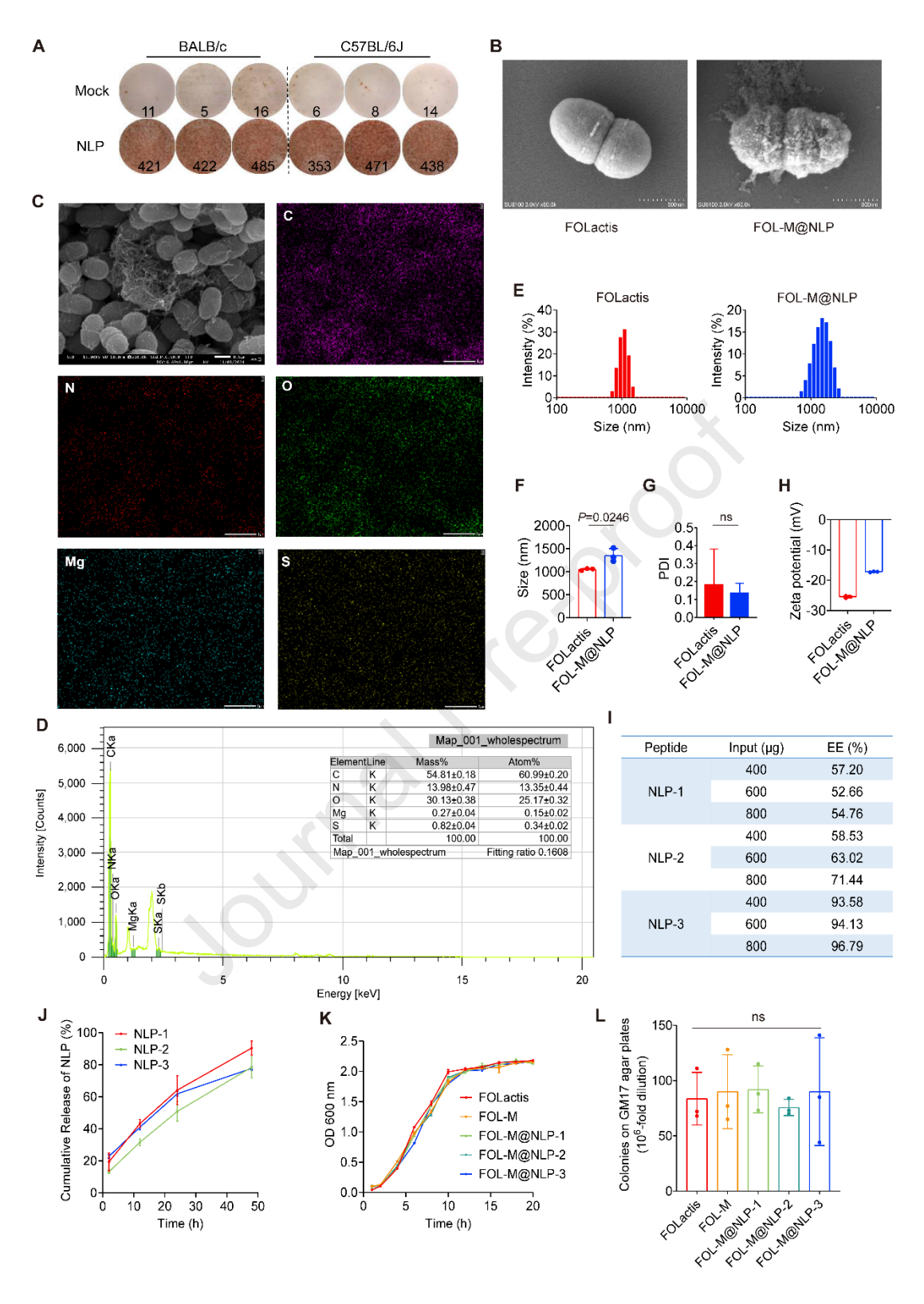


**Fig. 1.** Preparation and characterization of FOL-M@NLP. (A) IFN-γ secretion, assessed through ELISPOT assay, from splenocytes that underwent stimulation with 3 selected peptides from NY-ESO-1 (*n*=3). (B) Images of FOLactis and FOL-M@NLP

| captured by scanning electron microscopy (SEM), scale bar=500 nm. (C) Distributions            |
|--|
| of various elements on FOL-M@NLP determined by chemical mapping using energy                   |
| dispersive spectroscopy (EDS) in SEM, scale bar=1 μm. (D) Proportions of various               |
| elements determined by SEM/EDS. (E) Representative size distributions for FOLactis             |
| and FOL-M@NLP via dynamic light scattering. (F) Mean size of FOLactis and FOL-                 |
| M@NLP (n=3). (G) Polydispersity index of FOLactis and FOL-M@NLP (n=3). (H)                     |
| Zeta potential of FOLactis and FOL-M@NLP (n=3). (I) Encapsulation efficiencies of              |
| 3 selected peptides at different feeding doses. (J) Cumulative release of 3 selected           |
| peptides at different time points ( $n=3$ ). (K) Growth trajectories of FOLactis in different  |
| groups after activation. Optical density at 600 nm (OD600) were recorded at specified          |
| time intervals ( $n=3$ ). (L) Colonies grown from FOLactis in different groups on GM17         |
| agar plates containing chloramphenicol. The original bacterial suspension was coated           |
| on the plate after being diluted by $10^6$ folds ( $n=3$ ). The error bars represent the means |
| $\pm$ SD. Statistical significance was determined by analysis of $P$ values calculated via     |
| two-tailed unpaired Student's t tests or one-way ANOVA   |

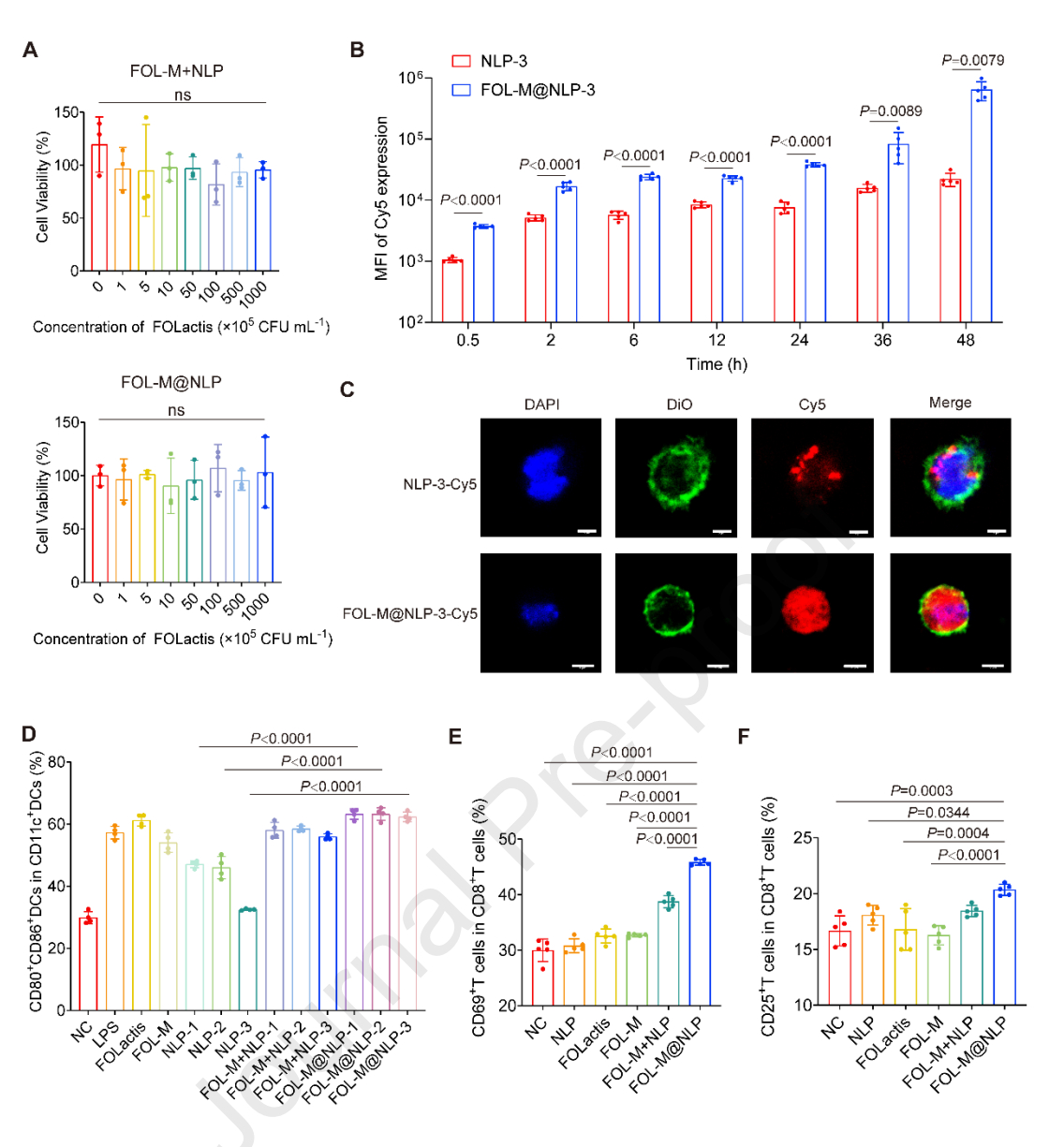


**Fig. 2.** *In vitro* immune response induced by FOL-M@NLP. (A) Cytotoxicity of FOL-M+NLP and FOL-M@NLP on BMDC (*n*=3). (B) Phagocytosis of NLP-3-Cy5 and FOL-M@NLP-3-Cy5 by BMDCs *in vitro* detected by flow cytometry at different durations (0.5 h, 2 h, 6 h, 12 h, 24 h, 36 h, and 48 h) (*n*=5). (C) Intracellular distributions of Cy5 in BMDCs after being incubated with NLP-3-Cy5 or FOL-M@NLP-3-Cy5 for 2 h. The BMDC nucleus was stained with DAPI (blue), the BMDC membrane was stained with DiO (green), and Cy5 expression in the peptides is shown in red. Intracellular distributions were detected using confocal microscopy. Scale bar=6 μm.

| (D) Flow cytometry statistics of mature DCs (CD11c <sup>+</sup> CD80 <sup>+</sup> CD86 <sup>+</sup> ) in BMDCs after                         |
|--|
| being coincubated with NLP, FOLactis, FOL-M, FOL-M+NLP, or FOL-M@NLP for   |
| 24 h. Blank 1640 medium was used as a negative control (NC), and LPS (2.5 $\mu g$ mL <sup>-1</sup> )   |
| was used as a positive control ( $n=4$ ). (E-F) Flow cytometry statistics of activated T cells   |
| (CD8 <sup>+</sup> CD69 <sup>+</sup> and CD8 <sup>+</sup> CD25 <sup>+</sup> ) in CD8 <sup>+</sup> T cells (n=5). T cells were cocultured with |
| BMDCs that incubated with NLP, FOLactis, FOL-M, FOL-M+NLP, and FOL-M@NLP   |
| previously. Blank 1640 medium was used as the NC. The error bars represent the means   |
| $\pm$ SD. Statistical significance was determined by analysis of $P$ values calculated via   |
| two-tailed unpaired Student's t tests or one-way ANOVA.  |
|  |

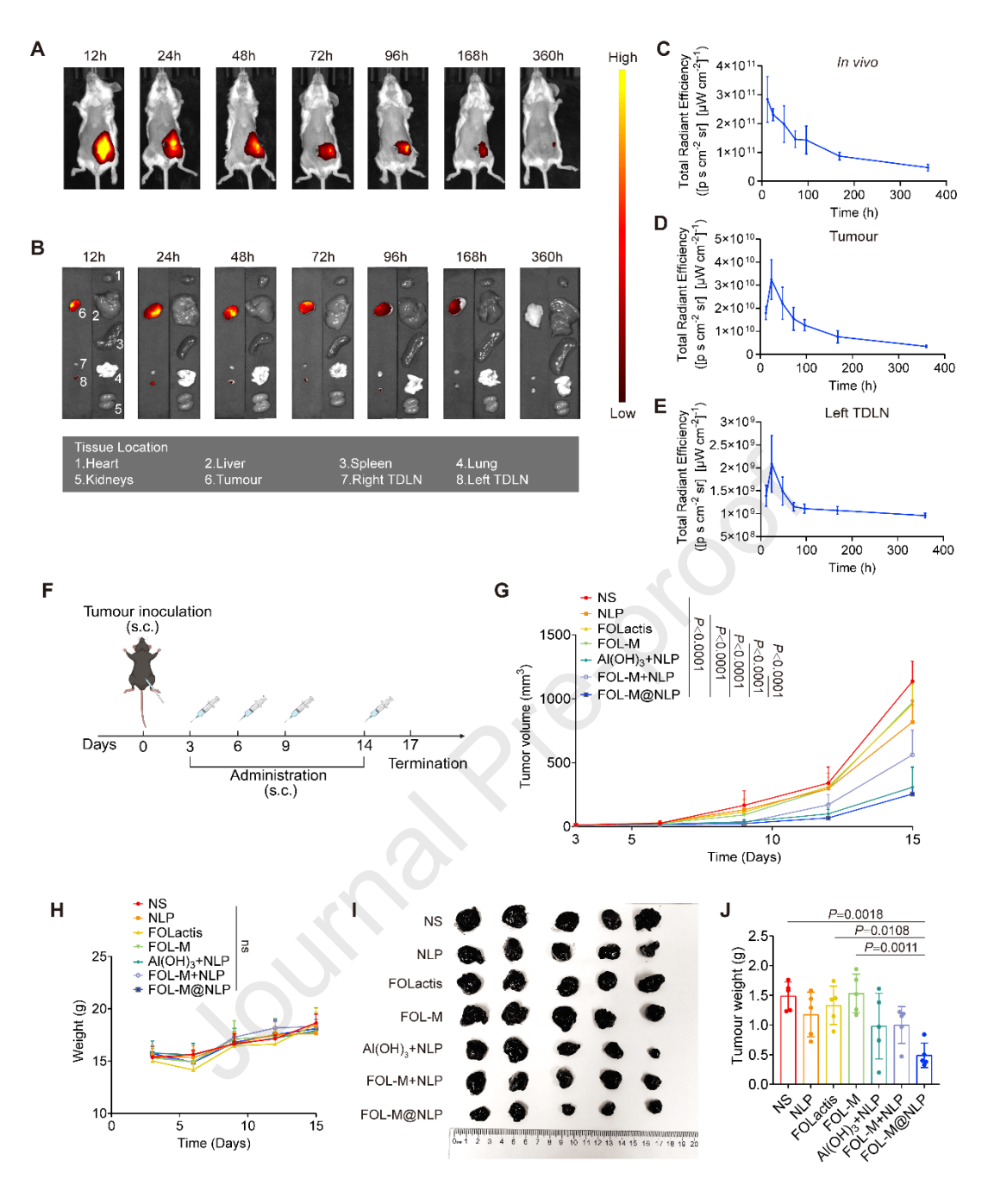


**Fig. 3.** Biodistribution and antitumour effect of FOL-M@NLP *in vivo*. (A) Biodistribution images of 4T1-NY-ESO-1 bearing mice following subcutaneous injection of FOL-M@NLP at different time intervals (n=4). (B) Biodistribution images of tumours, tumour-draining lymph nodes (TDLNs) and major organs harvested from 4T1-NY-ESO-1 bearing mice following subcutaneous injection of FOL-M@NLP at different time intervals (n=4). (C) Total radiant efficiency of FOL-M@NLP *in vivo* at

| different time intervals following subcutaneous injection ( $n=4$ ). (D) Total radiant |
|--|
| efficiency of FOL-M@NLP in tumours at different time intervals following               |
| subcutaneous injection ( $n=4$ ). (E) Total radiant efficiency of FOL-M@NLP in left    |
| TDLNs at different time intervals following subcutaneous injection ( $n=4$ ). (F)      |
| Schematic diagram of the therapeutic schedule for mice bearing B16F10-NY-ESO-1         |
| subcutaneous melanoma. Created in BioRender.com. (G) Tumour growth curves of           |
| B16F10-NY-ESO-1 tumour-bearing mice with different treatments ( $n=5$ ). (H) Weights   |
| of B16F10-NY-ESO-1 tumour-bearing mice during the therapeutic period $(n=5)$ . (I)     |
| Photographs of tumours harvested from mice in all groups on day 17 after tumour        |
| inoculation. (J) Weights of tumours harvested from mice in all groups on day 17 after  |
| tumour inoculation ( $n=5$ ). The error bars represent the means $\pm$ SD. Statistical |
| significance was determined by analysis of P values calculated via one-way ANOVA       |
| or two-way ANOVA.  |

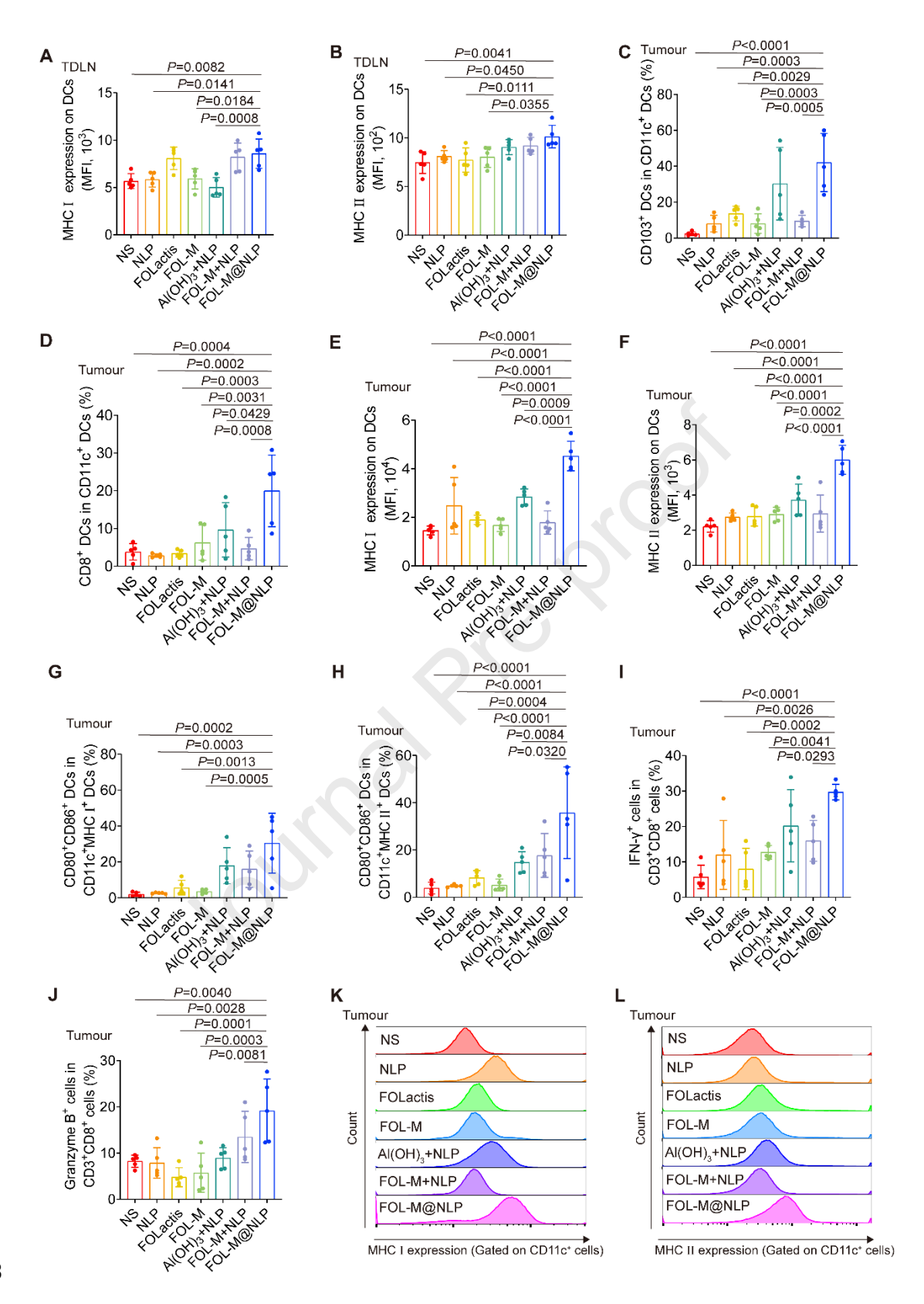


**Fig. 4.** Changes in immune microenvironment *in vivo* induced by FOL-M@NLP in primary B16F10-NY-ESO-1 melanoma model. (A) Flow cytometry statistics of MHC I expression on DCs in TDLNs of each group (*n*=5). (B) Flow cytometry statistics of

| MHC II expression on DCs in TDLNs of each group $(n=5)$ . (C) Flow cytometry  |
|---|
| statistics of CD103 <sup>+</sup> DCs (CD11c <sup>+</sup> CD103 <sup>+</sup> ) in tumours of each group ( <i>n</i> =5). (D) Flow |
| cytometry statistics of CD8 <sup>+</sup> DCs (CD11c <sup>+</sup> CD8 <sup>+</sup> ) in tumours of each group ( $n=5$ ). (E)     |
| Flow cytometry statistics of MHC I expression on DCs in tumours of each group $(n=5)$ .   |
| (F) Flow cytometry statistics of MHC II expression on DCs in tumours of each group  |
| (n=5). (G) Flow cytometry statistics of mature DCs expressing MHC I (CD11c <sup>+</sup> MHC                                     |
| I <sup>+</sup> CD80 <sup>+</sup> CD86 <sup>+</sup> ) in tumours of each group (n=5). (H) Flow cytometry statistics of           |
| mature DCs expressing MHC II (CD11c <sup>+</sup> MHC II <sup>+</sup> CD80 <sup>+</sup> CD86 <sup>+</sup> ) in tumours of each   |
| group ( $n=5$ ). (I) Flow cytometry statistics of IFN- $\gamma^+$ cytotoxic T cells (CD3 <sup>+</sup> CD8 <sup>+</sup> IFN-     |
| $\gamma^+$ ) in tumours of each group (n=5). (J) Flow cytometry statistics of granzyme B $^+$                                   |
| cytotoxic T cells (CD3 <sup>+</sup> CD8 <sup>+</sup> granzyme B <sup>+</sup> ) in tumours of each group (n=5). (K)              |
| Representative flow cytometry images of MHC I expression on DCs in tumours of each  |
| group. (L) Representative flow cytometry images of MHC II expression on DCs in  |
| tumours of each group. The error bars represent the means $\pm$ SD. Statistical significance                                    |
| was determined by analysis of P values calculated via one-way ANOVA.  |
|   |

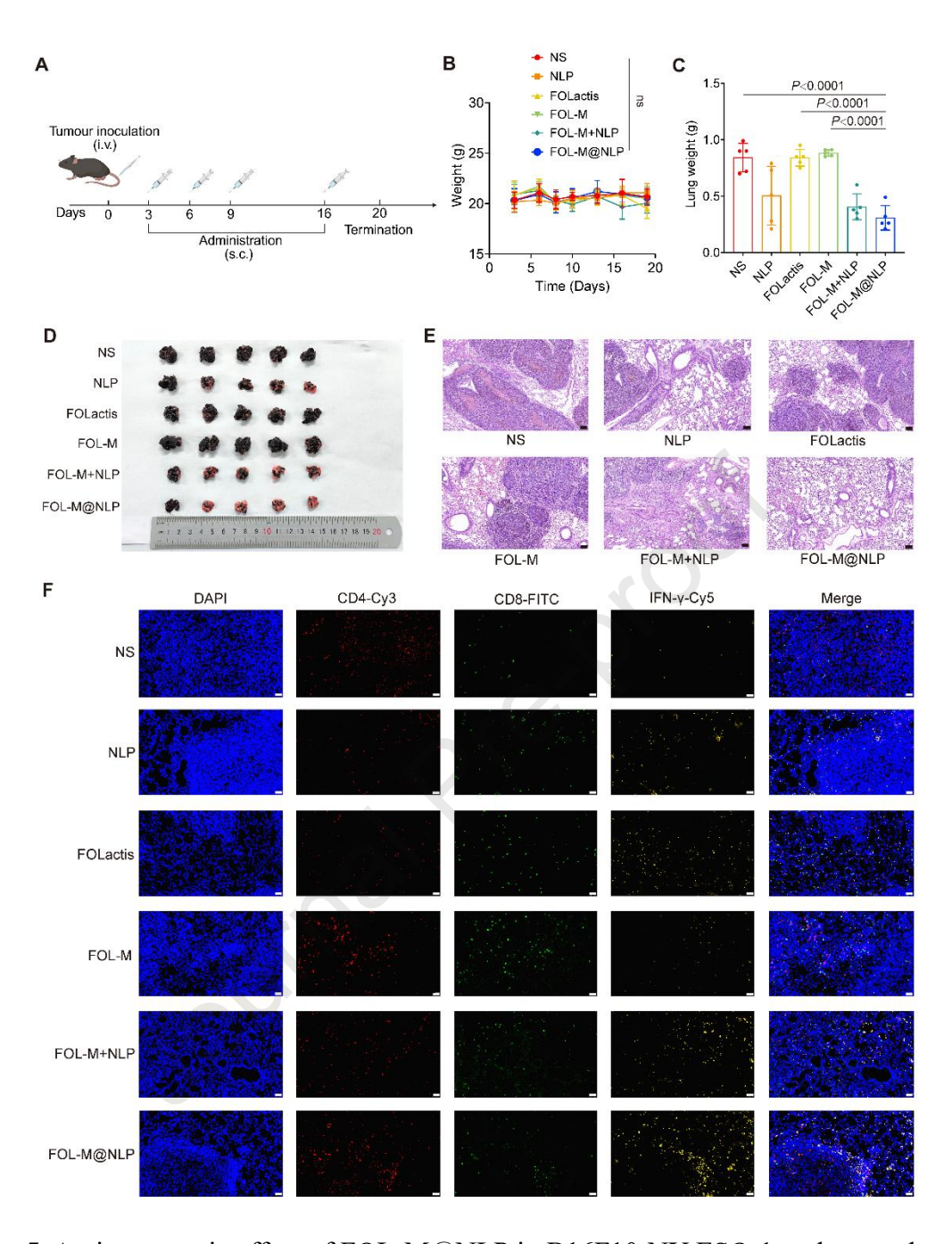
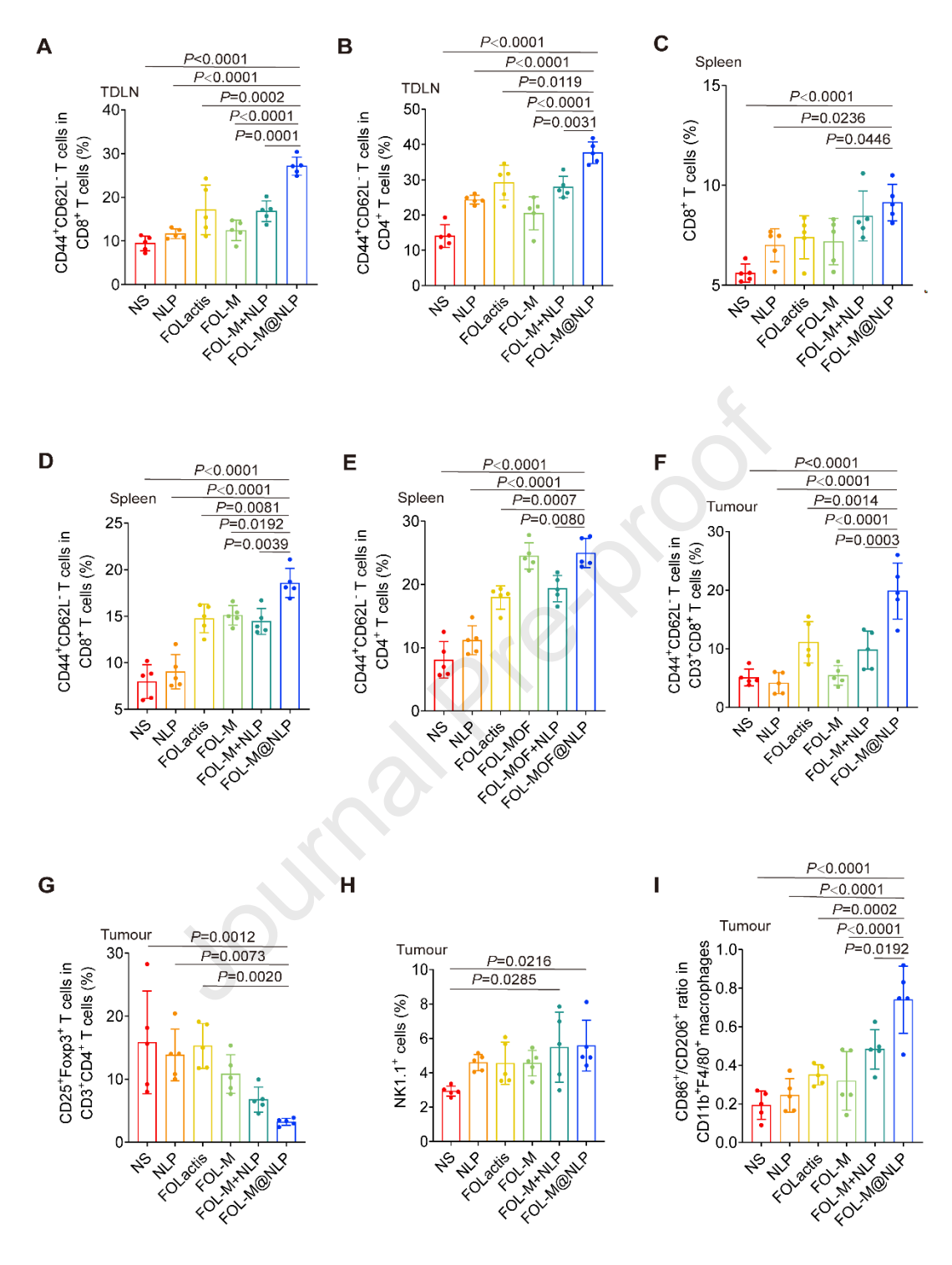


Fig. 5. Anti-metastatic effect of FOL-M@NLP in B16F10-NY-ESO-1 melanoma lung metastasis model. (A) Schematic diagram of the therapeutic schedule for mice bearing B16F10-NY-ESO-1 melanoma lung metastases. Created in BioRender.com. (B) Weights of B16F10-NY-ESO-1 metastasis-bearing mice during the therapeutic period (n=5). (C) Weights of lungs with metastatic lesions harvested from mice in all groups on day 20 after tumour inoculation (n=5). (D) Photographs of lungs with metastatic

| lesions harvested from mice in all groups on on day 20 after tumour inoculation. (E)                |
|---|
| Hematoxylin-eosin staining images of lungs with metastatic lesions harvested from                   |
| mice in all groups on day 20 after tumour inoculation. Scale bar=100 μm. (F)                        |
| Immunofluorescence images of CD4 $^+$ , CD8 $^+$ and IFN- $\gamma^+$ cells in lungs with metastatic |
| lesions harvested from mice in all groups on day 20 after tumour inoculation. Scale                 |
| bar=50 $\mu$ m. The error bars represent the means $\pm$ SD ( $n$ =5). Statistical significance was |
| determined by analysis of $P$ values calculated via one-way ANOVA.                                  |
|   |



**Fig. 6.** Changes in immune microenvironment *in vivo* induced by FOL-M@NLP in B16F10-NY-ESO-1 melanoma lung metastasis model. (A) Flow cytometry statistics of effector memory CD8<sup>+</sup> T cells (CD8<sup>+</sup>CD44<sup>+</sup>CD62L<sup>-</sup>) in TDLNs of each group (*n*=5).

(B) Flow cytometry statistics of effector memory CD4<sup>+</sup> T cells (CD4<sup>+</sup>CD44<sup>+</sup>CD62L<sup>-</sup>)

in TDLNs of each group (n=5). (C) Flow cytometry statistics of CD8<sup>+</sup> T cells in spleens 1087 of each group (n=5). (D) Flow cytometry statistics of effector memory CD8<sup>+</sup> T cells 1088  $(CD8^+CD44^+CD62L^-)$  in spleens of each group (n=5). (E) Flow cytometry statistics of 1089 effector memory CD4<sup>+</sup> T cells (CD4<sup>+</sup>CD44<sup>+</sup>CD62L<sup>-</sup>) in spleens of each group (*n*=5). 1090 1091 (F) Flow cytometry statistics of effector memory  $CD8^{+}$ T cells (CD3<sup>+</sup>CD8<sup>+</sup>CD44<sup>+</sup>CD62L<sup>-</sup>) in tumours of each group (n=5). (G) Flow cytometry 1092 statistics of regulatory T cells (CD3<sup>+</sup>CD4<sup>+</sup>CD25<sup>+</sup>FOXp3<sup>+</sup>) in tumours of each group 1093 (n=5). (H) Flow cytometry statistics of NK cells (NK1.1<sup>+</sup>) in tumours of each group 1094 (n=5). (I) Ratios of classically activated macrophages (CD11b+F4/80+CD86+) to 1095 alternatively activated macrophages (CD11b+F4/80+CD206+) detected by flow 1096 cytometry (n=5). The error bars represent the means  $\pm$  SD. Statistical significance was 1097 determined by analysis of P values calculated via one-way ANOVA. 1098

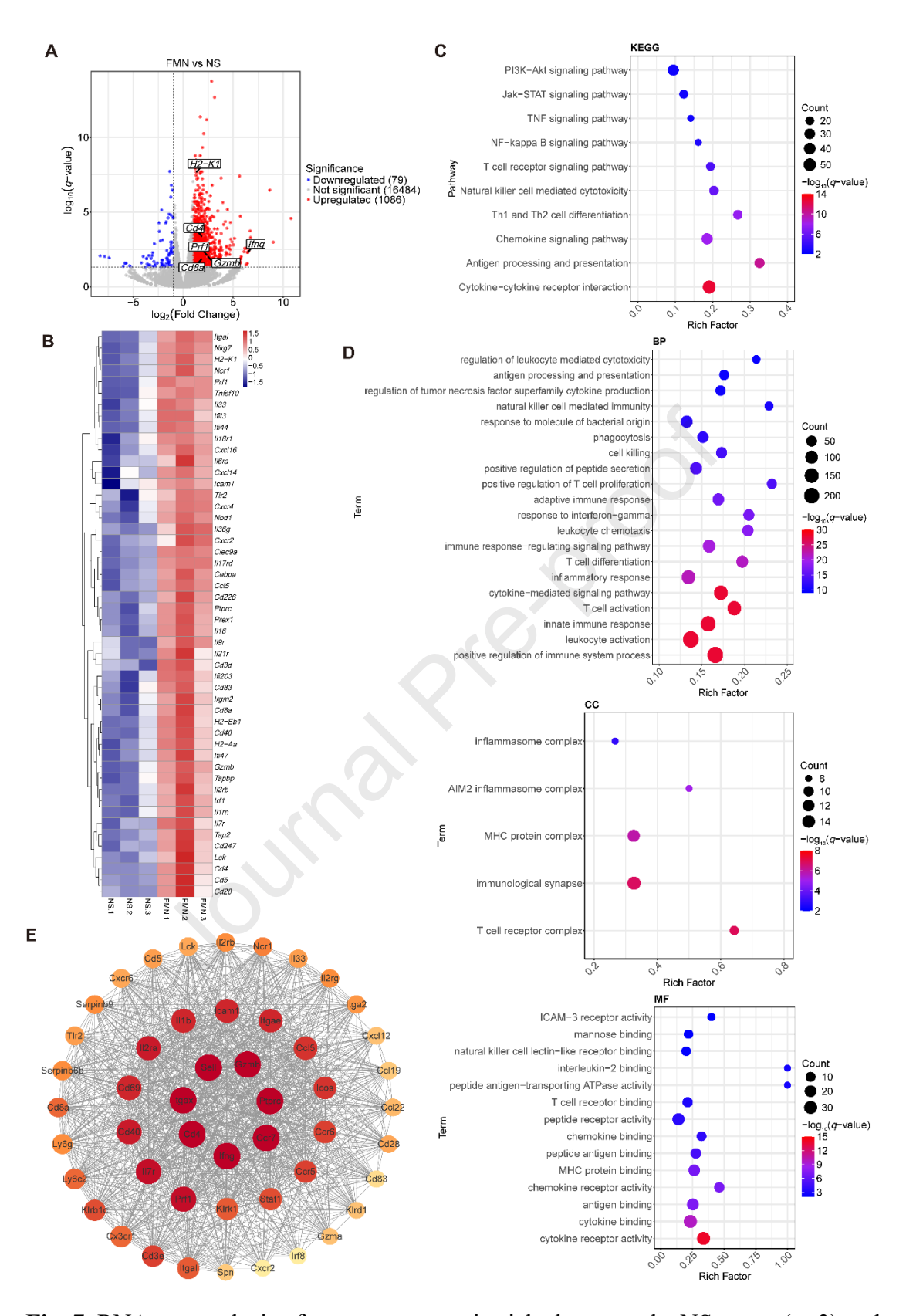


**Fig. 7.** RNA-seq analysis of tumour metastasis niche between the NS group (n=3) and the FOL-M@NLP group (FMN, n=3). (A) Volcano map of differentially expressed genes between the NS and FMN groups. The x-axis represents the log2 scale of the fold

| change in gene expression. Negative values indicate downregulation; positive values                  |
|--|
| indicate upregulation. The y-axis represents the minus $log_{10}$ scale of the q values (the         |
| adjusted $p$ values), indicating a significant difference in expression. The red dots                |
| represent significantly upregulated genes with at least $log_2(fold change) > 1$ and $q < 0.05$ ,    |
| whereas the blue dots represent significantly downregulated genes with at least                      |
| $\log_2(\text{fold change}) < -1$ and $q < 0.05$ . 6 representative genes related to key immune      |
| functions are displayed. (B) Heatmap of representative differentially expressed genes                |
| (DEGs) that play a positive role in the immune process. These genes were completely                  |
| clustered and were displayed from blue to white to red according to the $Z$ score from               |
| small to large. (C-D) KEGG pathway enrichment analysis and Gene Ontology (GO)                        |
| term enrichment analysis. GO enrichment analysis included analysis of biological                     |
| process (BP), cellular component (CC) and molecular function (MF) terms. The x-axis                  |
| represents the Rich factor. The y-axis represents the enriched pathways/terms. Changes               |
| in bubble size from small to large indicated that the number of DEGs in the                          |
| pathway/term changed from small to large. The changes in bubble color from blue to                   |
| red indicate that the $-\log_{10}(q \text{ value})$ changed from small to large. (E) Protein-protein |
| interaction (PPI) network of DEGs. Changes in the circle size from small to large                    |
| indicate that the betweenness changes from small to large. Changes in the brightness of              |
| a circle from light to dark indicate the degree changes from small to large. The central             |
| proteins were encoded by the hub genes.  |

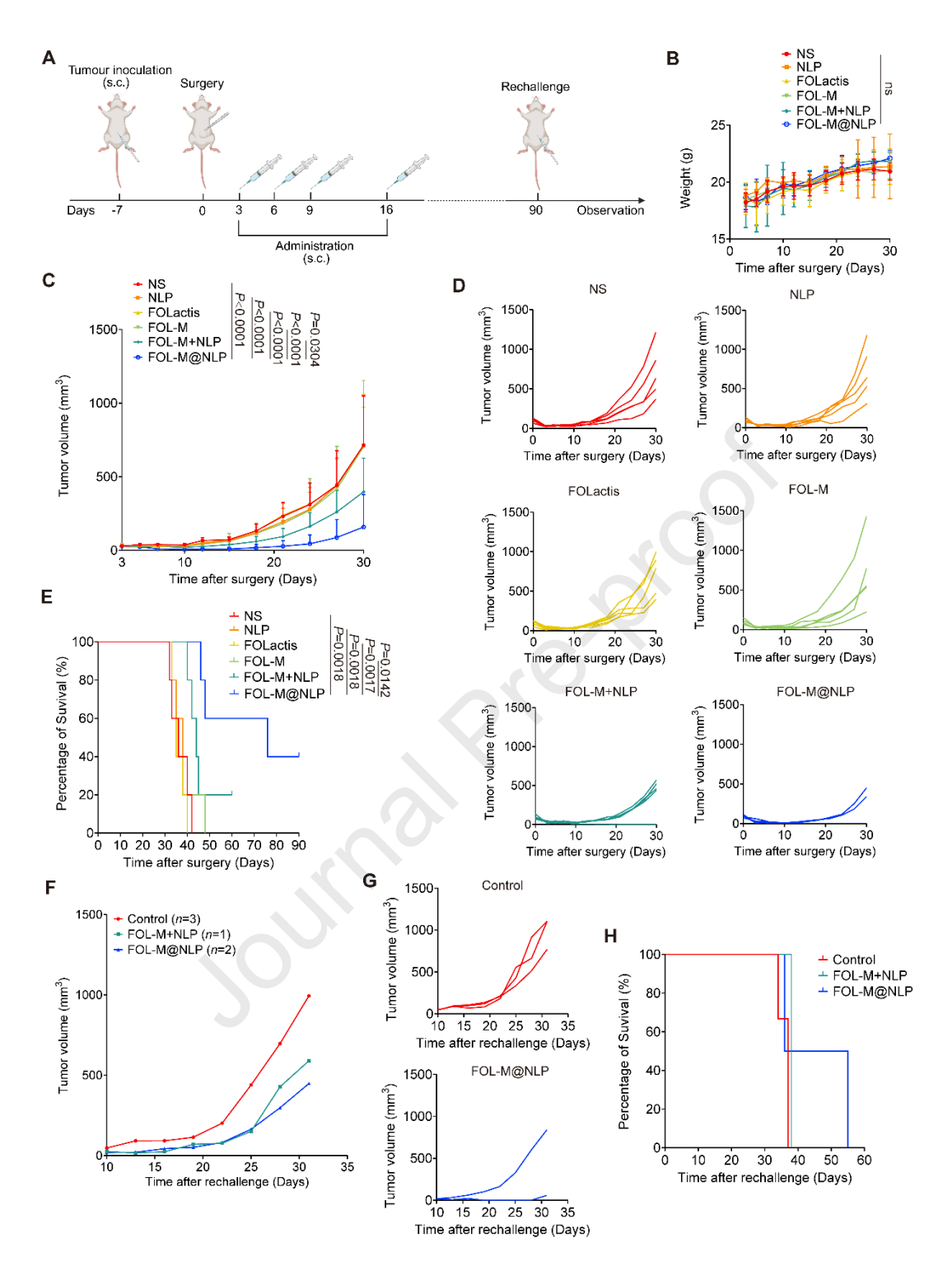
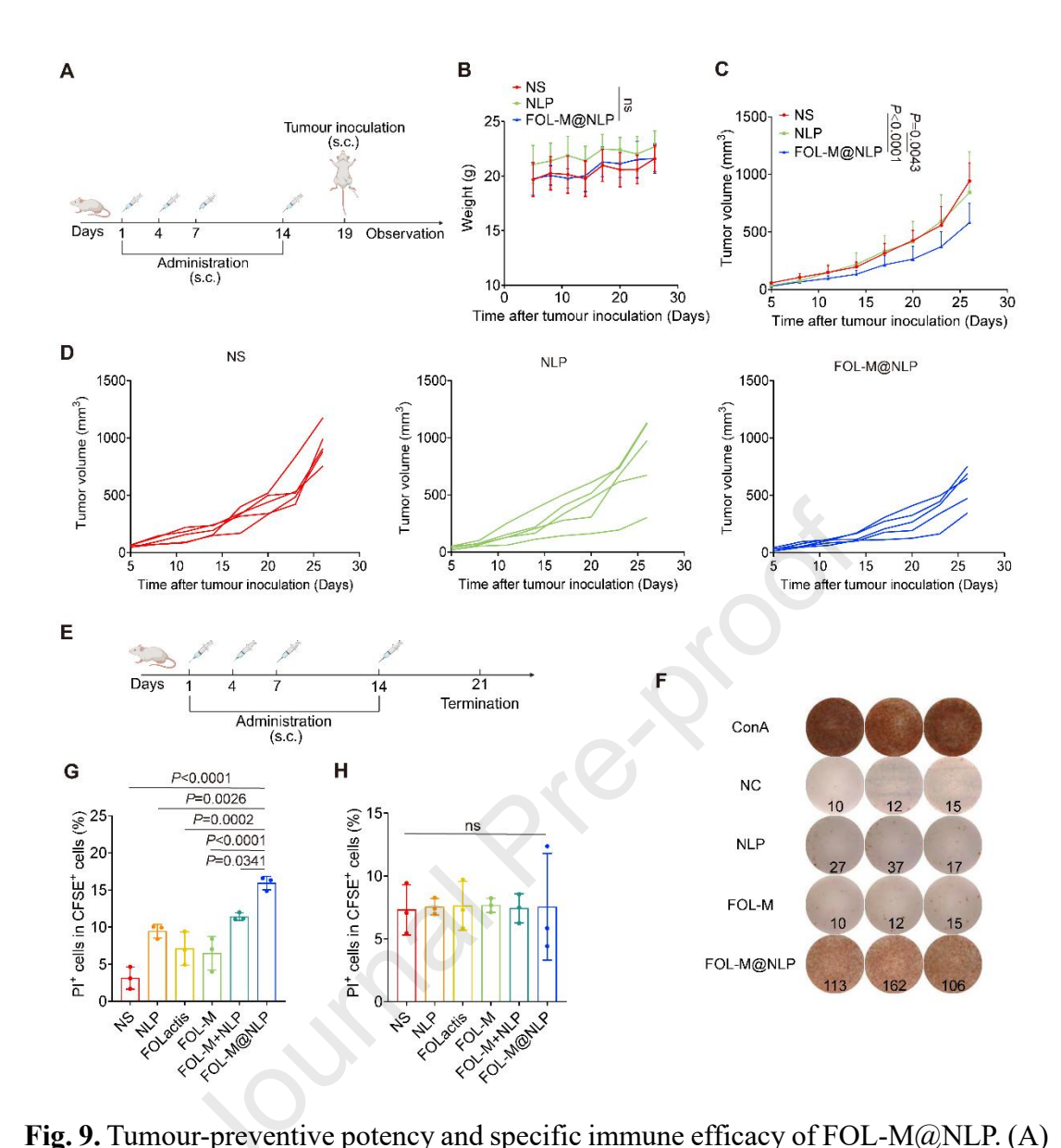


**Fig. 8.** Antitumour effect of FOL-M@NLP in breast cancer postoperative recurrence-preventing model. (A) Schematic diagram of the therapeutic schedule for mice bearing 4T1-NY-ESO-1 tumour. Created in BioRender.com. (B) Weights of mice from all groups during 30 days post-surgery (n=5). (C) Tumour growth curves of 4T1-NY-ESO-

| 1130 | 1 tumour-bearing mice with different treatments ( $n=5$ ). (D) Tumour growth curves of       |
|------|--|
| 1131 | each mouse in different groups ( $n=5$ ). (E) Survival curves of the different groups within |
| 1132 | 90 days after surgery ( $n=5$ ). (F) Tumour growth curves of mice in different groups after  |
| 1133 | rechallenge. (G) Tumour growth curves of each mouse in the control group and FOL-            |
| 1134 | M@NLP group. (H) Survival curves of different groups within 60 days after                    |
| 1135 | rechallenge. The error bars represent the means $\pm$ SD. Statistical significance was       |
| 1136 | determined by analysis of $P$ values calculated via two-way ANOVA or log-rank                |
| 1137 | (Mantel-Cox) test.   |
| 1138 |  |
| 1139 |  |
| 1140 |  |
| 1141 |  |
| 1142 |  |
| 1143 |  |



Schematic diagram of the vaccination schedule for mice before challenged with tumours. Created in BioRender.com (B) Weights of 4T1-NY-ESO-1 tumour-bearing mice from all groups following tumour inoculation (n=5). (C) Tumour growth curves of 4T1-NY-ESO-1 tumour-bearing mice from all groups following tumour inoculation (n=5). (D) Tumour growth curves of each mouse in different groups (n=5). (E) Schematic diagram of the vaccination schedule for mice. (F) IFN- $\gamma$  secretion, assessed through ELISPOT assay, from splenocytes that underwent different stimulation (n=3). (G) Flow cytometry statistics of destroyed 4T1-NY-ESO-1 cells (PI<sup>+</sup>) in CFSE<sup>+</sup> 4T1-

| L154 | NY-ESO-1 cells of each group ( $n=3$ ). (H) Flow cytometry statistics of destroyed wild- |
|------|--|
| 1155 | type 4T1 cells in CFSE $^+$ wild-type 4T1 cells of each group ( $n=3$ ). The error bars  |
| L156 | represent the means $\pm$ SD. Statistical significance was determined by analysis of $P$ |
| L157 | values calculated via one-way ANOVA or two-way ANOVA.                                    |
| L158 |  |
| L159 |  |
| 1160 |  |
|      |  |

# Highlights

- Long peptides screened from the NY-ESO-1 protein contain multiple epitopes with affinity for human and mouse major histocompatibility complexes I and II.
- The biovaccine FOL-M@NLP can be effectively taken up by antigen-presenting cells (APCs), then matures APCs and activates T lymphocytes *in vitro*.
- FOL-M@NLP effectively displays marked anti-tumour or preventive efficacy in various tumour models, enhance the expansion of immune cells in immune organs, improved the immune infiltrating state in tumours and activates innate and adaptive immune response adequately.
- The application of FOL-M@NLP induces specific cytotoxicity against target cells expressing NY-ESO-1 and exhibits favourable safety profiles.

| Dec | laration | of interests |  |
|-----|----------|--------------|--|
| DEC | iaralion | Of Interests |  |

| oxtimes The authors declare that they have no known competing financial interests or personal relationships that could have appeared to influence the work reported in this paper. |
|--|
| $\Box$ The authors declare the following financial interests/personal relationships which may be considered as potential competing interests:                                      |